

Two Higgs doublets with 4th generation fermions - models for TeV-scale compositeness

Shaouly Bar-Shalom*

Physics Department, Technion-Institute of Technology, Haifa 32000, Israel

Soumitra Nandi†

*Physique des Particules, Université de Montréal, C.P. 6128,
succ. centre-ville, Montréal, QC, Canada H3C 3J7*

Amarjit Soni‡

Theory Group, Brookhaven National Laboratory, Upton, NY 11973, USA

(Dated: January 26, 2013)

We construct a class of two Higgs doublets models with a 4th sequential generation of fermions that may effectively accommodate the low energy characteristics and phenomenology of a dynamical electroweak symmetry breaking scenario which is triggered by the condensates of the 4th family fermions. In particular, we single out the heavy quarks by coupling the “heavier” Higgs doublet (Φ_h) which possesses a much larger VEV only to them while the “lighter” doublet (Φ_ℓ) couples only to the light fermions. We study the constraints on these models from precision electroweak data as well as from flavor data. We also discuss some distinct new features that have direct consequences on the production and decays of the 4th family quarks and leptons in high energy colliders; in particular the conventional search strategies for t' and b' may need to be significantly revised.

PACS numbers:

I. INTRODUCTION

One of the most studied, yet unresolved theoretical puzzles in modern particle physics is the origin of ElectroWeak symmetry breaking (EWSB). Indeed, it is widely anticipated that the LHC will provide us with crucial answers regarding the underlying nature of EWSB: is the Higgs a fundamental scalar needing protection from SUSY or is it a composite object. In the Standard Model (SM), EWSB is triggered by the Higgs mechanism, which assumes a single fundamental scalar, the Higgs, with a mass at the EW-scale. This leads to the long standing difficulty known as the hierarchy problem: the presence of a fundamental EW-scale seems unnatural since there is a problem of stabilizing the Higgs mass against radiative corrections without introducing a cutoff to the theory at the nearby TeV scale. The hierarchy problem, which is usually being interpreted as evidence for new TeV-scale physics, has fueled much scientific effort in the past several decades, both in theory and in experiment.

Furthermore, recent flavor physics studies have revealed some degree of tension in the CKM fits for the SM with 3 generations [1–5]. For example, there are indications that the “predicted” value of $\sin 2\beta$ is larger than the value measured directly via the “gold-plated” ψK_s mode by as much as $\sim 3.3\sigma$ [6]. On the other hand, the announced CDF and DO results on the CP asymmetry $S_{\psi\phi}$ in $B_s \rightarrow \psi\phi$ (at a higher luminosity around 6/fb) are larger than the SM prediction by about 1σ [7], and at the same time, they find a surprisingly large CP-asymmetry in the same-sign dimuons signal, which they attribute primarily to a_{sl}^s - the semileptonic asymmetry in $B_s \rightarrow X_s \mu\nu$ [8, 9].

Interestingly, perhaps the simplest variant of the SM, known as the SM4, in which only a 4th sequential generation of fermion doublets is added to the theory (for reviews see [10–12]) can address some of the theoretical challenges associated with the hierarchy problem [13–15] and can readily account for the CKM anomalies mentioned above [16–24]. In particular, as was suggested over two decades ago, a heavy 4th generation fermion may trigger dynamical EWSB [13]. The picture that arises in this scenario is of new heavy fermions which have large Yukawa couplings that are driven to a Landau pole or a fixed point (which acts as a cutoff), possibly at the nearby TeV scale [14, 15]. Consequently, some form of strong dynamics and/or compositeness may occur and the Higgs particles are viewed as composites primarily of the 4th generation fermions (see e.g., [25–27]), with condensates $\langle Q'_L t'_R \rangle \neq 0$, $\langle Q'_L b'_R \rangle \neq 0$

*Electronic address: shaouly@physics.technion.ac.il

†Electronic address: soumitra.nandi@gmail.com

‡Electronic address: soni@bnl.gov

(and possibly also $\langle L'_L \nu'_R \rangle \neq 0$, $\langle L'_L \tau'_R \rangle \neq 0$), which induce EWSB and generate a dynamical mass for the condensing fermions. As for the CKM anomalies, the two extra phases that the SM4 possesses can give rise to a host of non-standard CP asymmetries [28, 29] and, in addition, can significantly ameliorate the difficulties with regard to baryogenesis that the SM has [28, 30, 31].

Indeed, recent searches for 4th generation heavy quarks by the CDF Collaboration have found that $m_{t'}, m_{b'} \gtrsim 350$ GeV [32] - in support of the compositeness scenario. Thus, any theory that contains these heavy fermionic states is inevitably cutoff at the near by TeV-scale where compositeness is expected to occur. As was realized already 20 years ago by Luty [33], the compositeness picture which emerges in this case may be more naturally embedded at low energies in multi-Higgs theories, since one should expect several composite scalars to emerge as manifestations of the different possible bound states of the fundamental heavy fermions. This idea was further studied recently in [27, 34–37]. Moreover, as will be shown in this paper, the addition of more scalar doublets relaxes the constraints from precision EW data (PEWD) (see also [36]), and allows for interesting new dynamics associated with the 4th generation fermions that can be tested at high energy colliders.

Adopting this viewpoint, in section II we construct a class of models with two scalar doublets and four generations of fermions that can serve as effective low energy frameworks and capture the key ingredients of the TeV-scale compositeness picture, by giving a special status to the heavy fermionic states. We then analyze in section III the constraints on these models from PEWD and from flavor physics in b-quark systems, and in section IV we discuss some of the new distinct phenomenological consequences of our multi-Higgs setup for collider searches of the 4th generation fermions. Finally, in section V we summarize our findings.

II. TWO HIGGS DOUBLET MODELS FOR THE 4TH GENERATION FERMIONS - 4G2HDMs

Recall that in a type II 2HDM (see [38]) one Higgs doublet couples only to the up-quarks while the 2nd Higgs doublet couples to the down-quarks. It is straight forward to extend such a setup to the case of a 4th generation fermion doublet - this was considered in [36, 39, 40] and within a SUSY framework in [30, 41–43].

Our aim here is to construct a new class of two Higgs doublet models (2HDMs) that can serve as a viable low energy effective framework for models of 4th generation condensation. Thus, in analogy with the 2HDM setup proposed in [44], we construct our 4G2HDMs using different Yukawa textures than the “standard” 2HDM of type II. In particular, in our 4G2HDMs one of the Higgs fields (call it the “heavier” field) couples only to heavy fermionic states, while the second Higgs field (the “lighter” field) is responsible for the mass generation of all other (lighter) fermions. In this way, the heavier field may be viewed as a $\bar{q}'q'$ composite with a condensate $\langle q'q' \rangle \neq 0$.

The Higgs potential is a general 2HDM one [38] and the Yukawa interaction Lagrangian of the quark sector is defined as:

$$\mathcal{L}_Y = -\bar{Q}_L \left(\Phi_\ell F \cdot \left(I - \mathcal{I}_d^{\alpha_d \beta_d} \right) + \Phi_h F \cdot \mathcal{I}_d^{\alpha_d \beta_d} \right) d_R - \bar{Q}_L \left(\tilde{\Phi}_\ell G \cdot \left(I - \mathcal{I}_u^{\alpha_u \beta_u} \right) + \Phi_h G \cdot \mathcal{I}_u^{\alpha_u \beta_u} \right) u_R + h.c. , \quad (1)$$

where $f_{L(R)}$ are left(right)-handed fermion fields, Q_L is the left-handed $SU(2)$ quark doublet and F, G are general 4×4 Yukawa matrices in flavor space. Also, $\Phi_{\ell, h}$ are the Higgs doublets:

$$\Phi_i = \begin{pmatrix} \phi_i^+ \\ \frac{v_i + \phi_i^0}{\sqrt{2}} \end{pmatrix}, \quad \tilde{\Phi}_i = \begin{pmatrix} \frac{v_i^* + \phi_i^{0*}}{\sqrt{2}} \\ -\phi_i^- \end{pmatrix},$$

I is the identity matrix and $\mathcal{I}_q^{\alpha_q \beta_q}$ ($q = d, u$) are diagonal 4×4 matrices defined by $\mathcal{I}_q^{\alpha_q \beta_q} \equiv \text{diag}(0, 0, \alpha_q, \beta_q)$.

The Yukawa texture of (1) can be realized in terms of a Z_2 -symmetry under which the fields transform as follows:

$$\begin{aligned} \Phi_\ell &\rightarrow -\Phi_\ell, \quad \Phi_h \rightarrow +\Phi_h, \quad Q_L \rightarrow +Q_L, \\ d_R &\rightarrow -d_R \quad (d = d, s), \quad u_R \rightarrow -u_R \quad (u = u, c), \\ b_R &\rightarrow (-1)^{1+\alpha_d} b_R, \quad b'_R \rightarrow (-1)^{1+\beta_d} b'_R, \\ t_R &\rightarrow (-1)^{1+\alpha_u} t_R, \quad t'_R \rightarrow (-1)^{1+\beta_u} t'_R. \end{aligned} \quad (2)$$

One can thus construct several models in which the Yukawa interactions of the heavy fermionic states have a non-trivial structure, possibly associated with the compositeness scenario. Three particularly interesting models which we will study in this paper are:

- **4G2HDM-I:** $(\alpha_d, \beta_d, \alpha_u, \beta_u) = (0, 1, 0, 1)$. In this case Φ_h gives masses only to t' and b' , while Φ_ℓ generates masses for all other quarks (including the top-quark).

- **4G2HDM-II:** $(\alpha_d, \beta_d, \alpha_u, \beta_u) = (1, 1, 1, 1)$. In this case the heavy condensate Φ_h is responsible for the mass generation of the heavy quarks states of both the 3rd and 4th generation quarks, whereas Φ_ℓ generates masses for the light quarks of the 1st and 2nd generations.
- **4G2HDM-III:** $(\alpha_d, \beta_d, \alpha_u, \beta_u) = (0, 1, 1, 1)$. In this case $m_t, m_{b'}, m_{t'} \propto v_h$, so that only quarks with masses at the EW-scale are coupled to the heavy doublet Φ_h .

The above 3 models represent, in our view, the minimal set of multi-Higgs frameworks that capture the compositeness scenarios associated with the heavy 4th generation fermions. Defining $\tan \beta \equiv v_h/v_\ell$, in the 4G2HDM-I we expect $\tan \beta \sim m_{q'}/m_t \sim \mathcal{O}(1)$ ($q' = t'$ or b'), while for the 4G2HDM-II and 4G2HDM-III models, $\tan \beta \gg 1$ seems to be a more natural choice.

As mentioned earlier, the construction of our 4G2HDM models was inspired in part by the 2HDM “for the top-quark”, which was introduced by Das and Kao in [44] and which was designed to give an effective explanation for the large top-quark mass via $v_h \gg v_\ell$. However, there is a fundamental difference between our 4G2HDMs and the Das and Kao 2HDM: the Das and Kao model which was constructed with three fermion generations has no new heavy fermions (the heavier Higgs doublet, Φ_h , couples only to the top-quark). Thus, without the new heavy fermionic degrees of freedom, the top-quark Yukawa coupling remains perturbative up to the Planck scale, so that their 2HDM does not have a natural low-energy cutoff as one would expect for the condensation picture. On the other hand, in our 4G2HDMs the strong Yukawa couplings of the heavier Higgs field to the new heavy 4th family fermions reaches a Landau pole at the near by TeV-scale, thus signaling new physics - possibly in the form of compositeness. Alternatively, our framework might be more naturally embedded into weakly coupled theories in 5 dimensions, see e.g., [25, 45].

From the point of view of the leptonic sector, the type-I 4G2HDM is the more natural underlying setup that can effectively accommodate the heavy masses of the 4th generation neutrino ν' . In particular, recall that the current bounds on $m_{\nu'}$ [49] indicate that ν' should have a mass at least at the EW-scale. The main glaring problem for the SM4 is the fact that it does not address the origin of such a heavy mass for ν' [48]. On the other hand, within our 4G2HDM-I the heaviness of the 4th generation leptons (with respect to the lighter three generations) is effectively accommodated by coupling them to the heavy Higgs doublet. This setup for the leptonic sector might also be an effective underlying description of more elaborate construction in models of warped extra dimensions, see e.g., [45].

The physical Higgs fields H^\pm and h, H, A (h and H are the lighter and heavier CP-even neutral states, respectively, and A is the neutral CP-odd state) are obtained by diagonalizing the neutral and charged Higgs mass matrices:

$$\begin{aligned}
\Phi_\ell^+ &= c_\beta G^+ - s_\beta H^+ , \\
\Phi_h^- &= s_\beta G^+ + c_\beta H^+ , \\
\Phi_\ell^0 &= c_\alpha H - s_\alpha h + i(c_\beta G^0 - s_\beta A) , \\
\Phi_h^0 &= s_\alpha H + c_\alpha h + i(s_\beta G^0 + c_\beta A) ,
\end{aligned} \tag{3}$$

where G^\pm, G^0 are the goldstone bosons, $c_\beta, s_\beta \equiv \cos \beta, \sin \beta$, $c_\alpha, s_\alpha \equiv \cos \alpha, \sin \alpha$ and α is the mixing angle in the CP-even neutral Higgs sector.

The Yukawa interactions between the physical Higgs bosons and quark states are then given by:

$$\mathcal{L}(hq_i q_j) = \frac{g}{2m_W} \bar{q}_i \left\{ m_{q_i} \frac{s_\alpha}{c_\beta} \delta_{ij} - \left(\frac{c_\alpha}{s_\beta} + \frac{s_\alpha}{c_\beta} \right) \cdot [m_{q_i} \Sigma_{ij}^q R + m_{q_j} \Sigma_{ji}^{q*} L] \right\} q_j h , \tag{4}$$

$$\mathcal{L}(Hq_i q_j) = \frac{g}{2m_W} \bar{q}_i \left\{ -m_{q_i} \frac{c_\alpha}{c_\beta} \delta_{ij} + \left(\frac{c_\alpha}{c_\beta} - \frac{s_\alpha}{s_\beta} \right) \cdot [m_{q_i} \Sigma_{ij}^q R + m_{q_j} \Sigma_{ji}^{q*} L] \right\} q_j H , \tag{5}$$

$$\mathcal{L}(Aq_i q_j) = -iI_q \frac{g}{m_W} \bar{q}_i \left\{ m_{q_i} \tan \beta \gamma_5 \delta_{ij} - (\tan \beta + \cot \beta) \cdot [m_{q_i} \Sigma_{ij}^q R - m_{q_j} \Sigma_{ji}^{q*} L] \right\} q_j A , \tag{6}$$

$$\begin{aligned}
\mathcal{L}(H^+ u_i d_j) &= \frac{g}{\sqrt{2}m_W} \bar{u}_i \left\{ [m_{d_j} \tan \beta \cdot V_{u_i d_j} - m_{d_k} (\tan \beta + \cot \beta) \cdot V_{ik} \Sigma_{kj}^d] R \right. \\
&\quad \left. + [-m_{u_i} \tan \beta \cdot V_{u_i d_j} + m_{u_k} (\tan \beta + \cot \beta) \cdot \Sigma_{ki}^{u*} V_{kj}] L \right\} d_j H^+ ,
\end{aligned} \tag{7}$$

where $q = d$ or u for down or up-quarks with weak Isospin $I_d = -\frac{1}{2}$ and $I_u = +\frac{1}{2}$, respectively, and $R(L) = \frac{1}{2}(1 + (-)\gamma_5)$. Also, V is the 4×4 CKM matrix and $\Sigma^d(\Sigma^u)$ are new mixing matrices in the down(up)-quark sectors, obtained after diagonalizing the quarks mass matrices:

$$\begin{aligned}\Sigma_{ij}^d &= \Sigma_{ij}^d(\alpha_d, \beta_d, D_R) = \alpha_d D_{R,3i}^* D_{R,3j} + \beta_d D_{R,4i}^* D_{R,4j}, \\ \Sigma_{ij}^u &= \Sigma_{ij}^u(\alpha_u, \beta_u, U_R) = \alpha_u U_{R,3i}^* U_{R,3j} + \beta_u U_{R,4i}^* U_{R,4j},\end{aligned}\quad (8)$$

where D_R, U_R are the rotation (unitary) matrices of the right-handed down and up-quarks, respectively. Notice that Σ^u and Σ^d depend only on the elements of the 3rd and 4th rows of U_R and D_R , respectively, and on whether α_q and/or β_q are “turned on”. For example, in model 4G2HDM-I, for which $(\alpha_d, \beta_d, \alpha_u, \beta_u) = (0, 1, 0, 1)$, only the 4th row elements of U_R and D_R are relevant.

Recall that in standard frameworks such as the single-Higgs SM4 or 2HDMs of types I and II [38], the right-handed mixing matrices U_R and D_R are non-physical in the sense that they are “rotated away” in the diagonalization procedure of the quark masses. On the other hand, in our 4G2HDMs some elements of these matrices can, in principle, be measured in Higgs-fermion systems, as we will later show. One can, thus, treat these matrices as unknowns, by expressing physical observables in terms of the elements of the 3rd and 4th rows of U_R and D_R , or study there properties under some theoretically motivated parameterization. In particular, inspired by the working assumption of our 4G2HDMs and by the observed flavor pattern in the up and down-quark sectors, we may assume the following structure (see also [44] for the 3×3 case):

$$D_R = \begin{pmatrix} \cos \theta_{ds} & -\sin \theta_{ds} & \sin \theta_{ds} \cos \theta_{bb'} \epsilon_s^* & -\cos \theta_{ds} \cos \theta_{bb'} \epsilon_s^* \\ \sin \theta_{ds} & \cos \theta_{ds} & -\sin \theta_{ds} \sin \theta_{bb'} \epsilon_s^* e^{-i\delta_b} & \cos \theta_{ds} \sin \theta_{bb'} \epsilon_s^* e^{-i\delta_b} \\ 0 & \epsilon_s & \cos \theta_{bb'} & -\sin \theta_{bb'} e^{-i\delta_b} \\ 0 & 0 & \sin \theta_{bb'} e^{i\delta_b} & \cos \theta_{bb'} \end{pmatrix}, \quad (9)$$

$$U_R = \begin{pmatrix} \cos \theta_{uc} & -\sin \theta_{uc} & \sin \theta_{uc} \cos \theta_{tt'} \epsilon_c^* & -\cos \theta_{uc} \cos \theta_{tt'} \epsilon_c^* \\ \sin \theta_{uc} & \cos \theta_{uc} & -\sin \theta_{uc} \sin \theta_{tt'} \epsilon_c^* e^{-i\delta_t} & \cos \theta_{uc} \sin \theta_{tt'} \epsilon_c^* e^{-i\delta_t} \\ 0 & \epsilon_c & \cos \theta_{tt'} & -\sin \theta_{tt'} e^{-i\delta_t} \\ 0 & 0 & \sin \theta_{tt'} e^{i\delta_t} & \cos \theta_{tt'} \end{pmatrix}, \quad (10)$$

where $\epsilon_s = \frac{m_s}{m_b} e^{i\delta_s}$ and $\epsilon_c = \frac{m_c}{m_t} e^{i\delta_c}$, so that unitarity of D_R and U_R is restored at 1st order in ϵ_s and ϵ_c , respectively. In the limit $\sin \theta_{uc} \sim m_u/m_c \ll 1$ and $\sin \theta_{ds} \sim m_d/m_s \ll 1$,^[1] U_R and D_R simplify to (similar textures can be found in Randall-Sundrum warped models of flavor [46, 47]):

$$D_R = \begin{pmatrix} 1 & 0 & 0 & -\epsilon_s^* \left(1 - \frac{|\epsilon_b|^2}{2}\right) \\ 0 & 1 & 0 & \epsilon_s^* \epsilon_b^* \\ 0 & \epsilon_s & \left(1 - \frac{|\epsilon_b|^2}{2}\right) & -\epsilon_b^* \\ 0 & 0 & \epsilon_b & \left(1 - \frac{|\epsilon_b|^2}{2}\right) \end{pmatrix}, \quad U_R = \begin{pmatrix} 1 & 0 & 0 & -\epsilon_c^* \left(1 - \frac{|\epsilon_t|^2}{2}\right) \\ 0 & 1 & 0 & \epsilon_c^* \epsilon_t^* \\ 0 & \epsilon_c & \left(1 - \frac{|\epsilon_t|^2}{2}\right) & -\epsilon_t^* \\ 0 & 0 & \epsilon_t & \left(1 - \frac{|\epsilon_t|^2}{2}\right) \end{pmatrix}, \quad (11)$$

where we have further defined

$$\epsilon_b = \sin \theta_{bb'} e^{i\delta_b}, \quad \epsilon_t = \sin \theta_{tt'} e^{i\delta_t}. \quad (12)$$

We thus obtain for the Σ mixing matrices in Eq. 8 (in each element keeping only the leading terms in ϵ_q , $q = s, c, b, t$):

$$\Sigma^d = \begin{pmatrix} 0 & 0 & 0 & 0 \\ 0 & \alpha_d |\epsilon_s|^2 & \alpha_d \epsilon_s^* \left(1 - \frac{|\epsilon_b|^2}{2}\right) & -\alpha_d \epsilon_s^* \epsilon_b^* \\ 0 & \alpha_d \epsilon_s \left(1 - \frac{|\epsilon_b|^2}{2}\right) & \alpha_d \left(1 - \frac{|\epsilon_b|^2}{2}\right) + \beta_d |\epsilon_b|^2 & (\beta_d - \alpha_d) \epsilon_b^* \left(1 - \frac{|\epsilon_b|^2}{2}\right) \\ 0 & -\alpha_d \epsilon_s \epsilon_b & (\beta_d - \alpha_d) \epsilon_b \left(1 - \frac{|\epsilon_b|^2}{2}\right) & \alpha_d |\epsilon_b|^2 + \beta_d \left(1 - \frac{|\epsilon_b|^2}{2}\right) \end{pmatrix}, \quad (13)$$

and similarly for Σ^u by replacing $\alpha_d, \beta_d \rightarrow \alpha_u, \beta_u$ and $\epsilon_s, \epsilon_b \rightarrow \epsilon_c, \epsilon_t$.

A natural choice which we will adopt in some instances below is: $|\epsilon_t| = \sin \theta_{tt'} \sim m_t/m_{t'}$ and $|\epsilon_b| = \sin \theta_{bb'} \sim m_b/m_{b'}$.

[1] The mixing angles θ_{uc} and θ_{ds} have no effect in our models as they enter only in the 1st and 2nd rows of U_R and D_R which have no physical outcome.

III. CONSTRAINTS ON THE 4G2HDMS

We now consider constraints from PEWD and from flavor physics in b-quark systems; namely $\bar{B} \rightarrow X_s \gamma$ and $B_q - \bar{B}_q$ ($q = d, s$) mixing. The PEWD constraints can be divided into the effects of the heavy new physics which does and does not couple directly to the SM ordinary fermions. For the former we consider constraints from $Z \rightarrow b\bar{b}$, which is mainly sensitive to the $H^+ t' b$ and $W^+ t' b$ couplings in our models. The effects which do not involve direct couplings to the ordinary fermions, are analyzed by the quantum oblique corrections to the gauge-bosons 2-point functions, which can be parameterized in terms of the oblique parameters S, T and U [50]. It should be noted that, as far as the oblique parameters are concerned, the contribution from our 4G2HDMS is identical at the 1-loop level to that of any 2HDM, since the new Hff Yukawa interactions in our models do not contribute at 1-loop to the gauge-bosons self energies.

A. $\bar{B} \rightarrow X_s \gamma$ and $B_q - \bar{B}_q$ mixing

1. $\bar{B} \rightarrow X_s \gamma$

The inclusive radiative decays of the B meson are known to be a very sensitive probe of new physics. Strong constraints on new physics from $\bar{B} \rightarrow X_s \gamma$ [51–53] crucially depend on theoretical uncertainties in the SM prediction for this decay. At the parton level, the decay process $B \rightarrow X_s \gamma$ is induced by the flavor changing (FC) decay of the b-quark into a strange quark.

The current experimental world average is given by [7],

$$\text{BR}[\bar{B} \rightarrow X_s \gamma] = (3.55 \pm 0.24 \pm 0.09) \times 10^{-4} . \quad (14)$$

In the SM, the calculation of the decay rate is most conveniently performed after decoupling the electroweak bosons and the top quark. In the resulting effective theory, the relevant FC weak interactions are given by a linear combination of dimension-five and -six operators [54]

$$\begin{aligned} O_{1,2} &= (\bar{s}\Gamma_i c)(\bar{c}\Gamma'_i b), & \text{(current-current operators)} \\ O_{3,4,5,6} &= (\bar{s}\Gamma_i b)\sum_q (\bar{q}\Gamma'_i q), & \text{(four-quark penguin operators)} \\ O_7 &= \frac{em_b}{16\pi^2} \bar{s}_L \sigma^{\mu\nu} b_R F_{\mu\nu}, & \text{(photonic dipole operator)} \\ O_8 &= \frac{gm_b}{16\pi^2} \bar{s}_L \sigma^{\mu\nu} T^a b_R G_{\mu\nu}^a. & \text{(gluonic dipole operator)} \end{aligned} \quad (15)$$

The Wilson coefficients, C_i , of these operators are perturbatively calculable at the renormalization scale $\mu_0 \sim (m_W, m_t)$ and the Renormalization Group Equations (RGE) can be used to evaluate C_i at the scale $\mu_b \sim m_b/2$. Finally, the operator on-shell matrix elements are calculated at μ_b . At present, all the relevant Wilson coefficients $C_i(\mu_b)$ are known at the Next-to-Next-to-Leading-Order (NNLO) [55–62]. However, the matrix elements of the operators O_i consists of perturbative and non-perturbative corrections. As far as the perturbative corrections are concerned, they are reduced dramatically after the completion of Next-to-Leading-Order (NLO) and NNLO QCD calculations. A further improvement comes from electroweak corrections [63–66]. On the other hand, no satisfactory quantitative estimates of all the non-perturbative effects are available, but they are believed to be $\approx 5\%$ [67].

In the SM within the leading log approximation, the $\bar{B} \rightarrow X_s \gamma$ amplitude is proportional to the (effective) Wilson coefficient of the operator O_7 . The well-known [68] expression for this coefficient reads

$$C_7^{(0)\text{eff}}(\mu_b) = \eta^{\frac{16}{23}} C_7^{(0)}(\mu_0) + \frac{8}{3} \left(\eta^{\frac{14}{23}} - \eta^{\frac{16}{23}} \right) C_8^{(0)}(\mu_0) + \sum_{i=1}^8 h_i \eta^{a_i}, \quad (16)$$

where $\eta = \alpha_s(\mu_0)/\alpha_s(\mu_b)$ and

$$h_i = \left(\frac{626126}{272277} - \frac{56281}{51730} - \frac{3}{7} - \frac{1}{14} - 0.6494 - 0.0380 - 0.0185 - 0.0057 \right) . \quad (17)$$

Separating the charm and top contributions, and neglecting the CKM-suppressed u -quark contribution, eq. (16) can be written as [69]

$$C_7^{(0)\text{eff}}(\mu_b) = X_c + X_t, \quad (18)$$

where the charm contribution, given by X_c , is obtained from eq. (16) by the replacement: $C_7^{(0)}(\mu_0) \rightarrow -\frac{23}{36}$ and $C_8^{(0)}(\mu_0) \rightarrow -\frac{1}{3}$,

$$X_c = -\frac{23}{36}\eta^{\frac{16}{23}} - \frac{8}{9}\left(\eta^{\frac{14}{23}} - \eta^{\frac{16}{23}}\right) + \sum_{i=1}^8 h_i \eta^{a_i}, \quad (19)$$

which is equivalent to including only charm contributions to the matching conditions for the corresponding operators. Analogously, only the top-loop contributes to X_t and the expression is given by

$$X_t = -\frac{1}{2}A_0^t(x_t)\eta^{\frac{16}{23}} - \frac{4}{3}F_0^t(x_t)\left(\eta^{\frac{14}{23}} - \eta^{\frac{16}{23}}\right), \quad (20)$$

with $x_t \equiv (m_t(\mu_0)/m_W)^2$ and

$$\begin{aligned} A_0^t(x) &= \frac{-3x^3+2x^2}{2(x-1)^4} \ln x + \frac{-22x^3+153x^2-159x+46}{36(x-1)^3}, \\ F_0^t(x) &= \frac{3x^2}{2(x-1)^4} \ln x + \frac{-5x^3+9x^2-30x+8}{12(x-1)^3}. \end{aligned}$$

Including the perturbative, electroweak and the available non-perturbative corrections, the branching ratio of $\bar{B} \rightarrow X_s \gamma$, with an energy cut-off E_0 in the \bar{B} -meson rest frame, can be written as follows [69]:

$$\text{BR}[\bar{B} \rightarrow X_s \gamma]_{E_\gamma > E_0}^{\text{subtracted } \psi, \psi'} = \text{BR}[\bar{B} \rightarrow X_c e \bar{\nu}]_{\text{exp}} \left| \frac{V_{ts}^* V_{tb}}{V_{cb}} \right|^2 \frac{6\alpha_{\text{em}}}{\pi C} [P(E_0) + N(E_0)], \quad (21)$$

where $\alpha_{\text{em}} = \alpha_{\text{em}}^{\text{on shell}}$ [64], $N(E_0)$ denotes the non-perturbative correction and $P(E_0)$ is given by the perturbative ratio

$$\frac{\Gamma[b \rightarrow X_s \gamma]_{E_\gamma > E_0}}{|V_{cb}/V_{ub}|^2 \Gamma[b \rightarrow X_u e \bar{\nu}]} = \left| \frac{V_{ts}^* V_{tb}}{V_{cb}} \right|^2 \frac{6\alpha_{\text{em}}}{\pi} P(E_0). \quad (22)$$

In their approach (see [69]) the *charmless* semileptonic rate has been chosen as the normalization factor in eq. (22), whereas C in eq. (21) is given by

$$C = \left| \frac{V_{ub}}{V_{cb}} \right|^2 \frac{\Gamma[\bar{B} \rightarrow X_c e \bar{\nu}]}{\Gamma[\bar{B} \rightarrow X_u e \bar{\nu}]}. \quad (23)$$

Furthermore, the perturbative quantity $P(E_0)$ can be written as [69]:

$$P(E_0) = \left| K_c + \left(1 + \frac{\alpha_s(\mu_0)}{\pi} \ln \frac{\mu_0^2}{m_t^2} \right) r(\mu_0) K_t + \varepsilon_{\text{ew}} \right|^2 + B(E_0), \quad (24)$$

where K_t contains the top-quark contribution to the $b \rightarrow s \gamma$ amplitude and K_c contains the remaining contributions, among which the charm loops are by far the dominant one. Also, the electroweak correction to the $b \rightarrow s \gamma$ amplitude is denoted in Eq. 24 by ε_{ew} and $B(E_0)$ is the bremsstrahlung function which contains the effects of $b \rightarrow s \gamma g$ and $b \rightarrow s \gamma q \bar{q}$ ($q = u, d, s$) transitions and which is the only E_0 -dependent part in $P(E_0)$.

The NLO expression for K_t is given by [69]

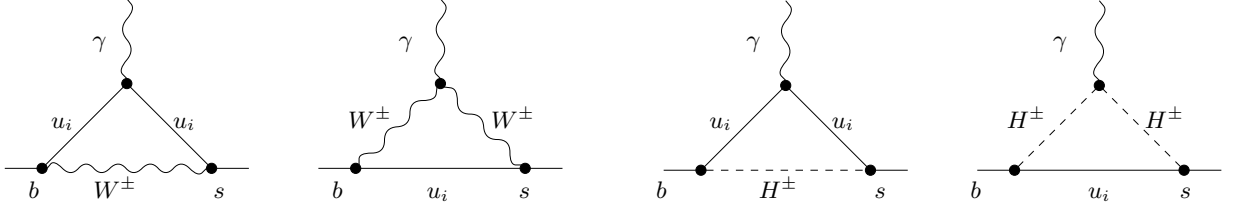


FIG. 1: Examples of one-loop 1PI diagrams that contribute to $b \rightarrow s\gamma$ in the 4G2HDM, with W -bosons, charged Higgs and 4th generation quarks exchanges ($u_i = u, c, t, t'$).

$$\begin{aligned}
K_t = & \left[1 - \frac{2}{9}\alpha_s(m_b)^2 + \frac{\alpha_s(\mu_0)}{\pi} \ln \frac{\mu_0}{m_t} 4x \frac{\partial}{\partial x} \right] \left[-\frac{1}{2}\eta^{\frac{4}{23}} A_0(x_t) + \frac{4}{3} \left(\eta^{\frac{4}{23}} - \eta^{\frac{2}{23}} \right) F_0(x_t) \right] \\
& + \frac{\alpha_s(\mu_b)}{4\pi} \left\{ E_0(x_t) \sum_{k=1}^8 e_k \eta^{(a_k + \frac{11}{23})} \right. \\
& + \eta^{\frac{4}{23}} \left[-\frac{1}{2}\eta A_1(x_t) + \left(\frac{12523}{3174} - \frac{7411}{4761}\eta - \frac{2}{9}\pi^2 - \frac{4}{3} \left(\ln \frac{m_b}{\mu_b} + \eta \ln \frac{\mu_0}{m_t} \right) \right) A_0(x_t) \right. \\
& \quad \left. + \frac{4}{3}\eta F_1(x_t) + \left(-\frac{50092}{4761} + \frac{1110842}{357075}\eta + \frac{16}{27}\pi^2 + \frac{32}{9} \left(\ln \frac{m_b}{\mu_b} + \eta \ln \frac{\mu_0}{m_t} \right) \right) F_0(x_t) \right] \\
& \left. + \eta^{\frac{2}{23}} \left[-\frac{4}{3}\eta F_1(x_t) + \left(\frac{2745458}{357075} - \frac{38890}{14283}\eta - \frac{4}{9}\pi(\pi + i) - \frac{16}{9} \left(\ln \frac{m_b}{\mu_b} + \eta \ln \frac{\mu_0}{m_t} \right) \right) F_0(x_t) \right] \right\}, \quad (25)
\end{aligned}$$

where the functions $A_1^t(x)$ and $F_1^t(x)$ and the expression for K_c are given in Ref. [69].

For the electroweak (ε_{ew}) and non-perturbative ($N(E_0)$) corrections in eq. (21) we consider the following values [69],

$$\begin{aligned}
\varepsilon_{\text{ew}} & \approx 0.0035 + 0.0012 + 0.0028 = 0.0075 \\
N(E_0) & = 0.0036 \pm 0.0006. \quad (26)
\end{aligned}$$

Other required inputs which we take from [69] are,

$$r(\mu_0 = m_t) = 0.578 \pm 0.002_{\mu_b} \pm (\text{parametric errors}) \quad (27)$$

$$C = 0.575 (1 \pm 0.01 \pm 0.02 \pm 0.02) \quad (28)$$

$$a(z) = (0.97 \pm 0.25) + i(1.01 \pm 0.15) \quad (29)$$

$$b(z) = (-0.04 \pm 0.01) + i(0.09 \pm 0.02), \quad (30)$$

where $a(z)$ and $b(z)$ are the z -dependent terms in K_c ($z = (m_c/m_b)^2$, see Eq. 3.7 in [69]).

With these inputs the NLO prediction for the branching fraction of $B \rightarrow X_s \gamma$ is [69]

$$\text{BR}[\bar{B} \rightarrow X_s \gamma]_{E_\gamma > 1.6 \text{ GeV}} = (3.60 \pm 0.30) \times 10^{-4}. \quad (31)$$

In the SM4 there are no new operators other than the ones present in the SM. However, there are extra contributions to the Wilson coefficients corresponding to the operators O_7 and O_8 from t' -loop [16–19]. In our 4G2HDMs the new ingredient with respect to the SM4 is the presence of the charged Higgs which gives new contributions to the Wilson coefficients of the effective theory. Examples of the 1-loop diagrams that contribute to $b \rightarrow s\gamma$ in our 4G2HDMs are given in Fig. 1.^[2]

In order to include the charged-Higgs effect we need to compute the new Wilson coefficients at the matching scale μ_0 (The new $H^\pm u_i d_j$ Yukawa interactions in our models are given in Eq. 7). At the LO, the charged-Higgs contributions, with the t -quark in the loops are given by (see also [70]),

$$\delta C_i^{(0)eff}(\mu_0) = 0 \quad i = 1, \dots, 6 \quad (32)$$

[2] We are considering only the charged Higgs contributions to $b \rightarrow s\gamma$ and neglecting the flavor changing neutral Higgs 1-loop exchanges, which are much smaller in our models due to the very small $b-s$ and $b'-s$ transitions as embedded in Σ^d (see Eq. 13).

$$\delta C_{7,8}^{(0)eff}(\mu_0) = \frac{A_{U_t}}{3} F_{7,8}^{(1)}(y_t) + A_{D_t} F_{7,8}^{(2)}(y_t), \quad (33)$$

and that of t' in the loops are given by

$$\delta C_{7,8}^{(0)'eff}(\mu_0) = \frac{A_{U_{t'}}}{3} F_{7,8}^{(1)}(y_{t'}) + A_{D_{t'}} F_{7,8}^{(2)}(y_{t'}) , \quad (34)$$

where $y_i = \frac{\bar{m}_i^2(\mu_0)}{m_{H^+}^2}$, and the functions $F_{7,8}^{(1,2)}(y_i)$ are given by [51, 53, 70]

$$\begin{aligned} F_7^{(1)}(y_i) &= \frac{y_i(7-5y_i-8y_i^2)}{24(y_i-1)^3} + \frac{y_i^2(3y_i-2)}{4(y_i-1)^4} \ln y_i, \\ F_8^{(1)}(y_i) &= \frac{y_i(2+5y_i-y_i^2)}{8(y_i-1)^3} - \frac{3y_i^2}{4(y_i-1)^4} \ln y_i, \\ F_7^{(2)}(y_i) &= \frac{y_i(3-5y_i)}{12(y_i-1)^2} + \frac{y_i(3y_i-2)}{6(y_i-1)^3} \ln y_i, \\ F_8^{(2)}(y_i) &= \frac{y_i(3-y_i)}{4(y_i-1)^2} - \frac{y_i}{2(y_i-1)^3} \ln y_i . \end{aligned} \quad (35)$$

Dropping terms proportional to m_s (the strange-quark mass) and also neglecting the terms proportional to $\Sigma_{bb} \propto |\epsilon_b|^2$ (which is expected to be small compared to the leading terms), the factors $A_{U_{t/t'}}$ and $A_{D_{t/t'}}$ in Eqs. 33 and 34 are given by

$$\begin{aligned} A_{U_t} &= (A_{u_1} - A_{u_2} \Sigma_{tt})^2 + \sqrt{\frac{y_t}{y_{t'}}} \left(\frac{V_{t's}^*}{V_{ts}^*} + \frac{V_{t'b}}{V_{tb}} \right) \Sigma_{t't} (A_{u_2}^2 \Sigma_{tt} - A_{u_1} A_{u_2}) + \frac{y_{t'}}{y_t} \frac{\lambda_{sb}^{t'}}{\lambda_{sb}^t} A_{u_2}^2 \Sigma_{t't}^2, \\ A_{D_t} &= -A_{d_1} A_{u_1} + A_{d_1} A_{u_2} \Sigma_{tt} + \frac{m_{b'}}{m_b} \frac{V_{tb'}}{V_{tb}} (A_{d_2} A_{u_1} - A_{d_2} A_{u_2} \Sigma_{tt}) \Sigma_{b'b} \\ &\quad - \sqrt{\frac{y_{t'}}{y_t}} \frac{m_{b'}}{m_b} \frac{\lambda_{bs}^{t'}}{\lambda_{bs}^t} A_{u_2} A_{d_2} \Sigma_{t't} \Sigma_{b'b} + \sqrt{\frac{y_{t'}}{y_t}} \frac{V_{t's}^*}{V_{ts}^*} A_{d_1} A_{u_2} \Sigma_{t't}, \\ A_{U_{t'}} &= (A_{u_1} - A_{u_2} \Sigma_{t't'})^2 + \sqrt{\frac{y_t}{y_{t'}}} \left(\frac{V_{ts}^*}{V_{t's}^*} + \frac{V_{tb}}{V_{t'b}} \right) \Sigma_{tt'} (A_{u_2}^2 \Sigma_{t't'} - A_{u_1} A_{u_2}) + \frac{y_t}{y_{t'}} \frac{\lambda_{sb}^t}{\lambda_{sb}^{t'}} A_{u_2}^2 \Sigma_{t't'}^2, \\ A_{D_{t'}} &= -A_{d_1} A_{u_1} + A_{d_1} A_{u_2} \Sigma_{t't'} + \frac{m_{b'}}{m_b} \frac{V_{t'b'}}{V_{t'b}} (A_{d_2} A_{u_1} - A_{d_2} A_{u_2} \Sigma_{t't'}) \Sigma_{b'b} \\ &\quad - \sqrt{\frac{y_t}{y_{t'}}} \frac{m_{b'}}{m_b} \frac{\lambda_{bs}^t}{\lambda_{bs}^{t'}} \frac{V_{t'b'}}{V_{tb}} A_{u_2} A_{d_2} \Sigma_{t't} \Sigma_{b'b} + \sqrt{\frac{y_t}{y_{t'}}} \frac{V_{ts}^*}{V_{t's}^*} A_{d_1} A_{u_2} \Sigma_{t't'}. \end{aligned} \quad (36)$$

where for later convenience we have defined

$$A_{u_1} = A_{d_1} = \tan \beta, \quad A_{u_2} = A_{d_2} = \tan \beta + \cot \beta. \quad (37)$$

In all the cases where the new physics contributions do not involve new operators (and in which $C_k^{\text{new}}(\mu_0) = 0$ for $k = 1, 2, 3, 5, 6$ as in our case - see Eq. 32), it is straightforward to incorporate the extra terms to the NLO formulae. In particular, these contributions effectively modify K_t given in Eq. 24, which in our 4G2HDMs should be replaced by

$$K_t \rightarrow K_t^W + \frac{V_{t'b} V_{t's}^*}{V_{tb} V_{ts}^*} K_{t'}^W + K_t^H + \frac{V_{t'b} V_{t's}^*}{V_{tb} V_{ts}^*} K_{t'}^H, \quad (38)$$

where K_t^W , $K_{t'}^W$, K_t^H and $K_{t'}^H$ represent the W and charged-Higgs contributions to the $b \rightarrow s\gamma$ amplitudes from t and t' loops (see Fig. 1). In particular, $K_{t'}^W$ can be obtained simply by replacing (neglecting $\ln(\frac{\mu_0}{m_t})$)

$$\begin{aligned} E_0(x_t) &\rightarrow E_0(x_{t'}), \\ A_0(x_t) &\rightarrow A_0(x_{t'}), \\ A_1(x_t) &\rightarrow A_1(x_{t'}), \\ F_0(x_t) &\rightarrow F_0(x_{t'}), \\ F_1(x_t) &\rightarrow F_1(x_{t'}), \end{aligned} \quad (39)$$

in eq. 25. On the other hand, K_t^H and $K_{t'}^H$, which represent the net contributions to the $b \rightarrow s\gamma$ amplitude from charged-Higgs exchanges (with t and t' as the internal quark, respectively), can be obtained from Eq. 25 by calculating the functions $E_0(y_i)$, $A_0(y_i)$, $A_1(y_i)$, $F_0(y_i)$ and $F_1(y_i)$ ($i = t$ or $i = t'$). The LO functions $A_0(y_t)$ and $A_0(y_{t'})$ are given by

$$\begin{aligned} A_0(y_t) &= -2 \delta C_7^{(0)eff}(\mu_0), & F_0(y_t) &= -2 \delta C_8^{(0)eff}(\mu_0), \\ A_0(y_{t'}) &= -2 \delta C_7^{(0)'eff}(\mu_0), & F_0(y_{t'}) &= -2 \delta C_8^{(0)'eff}(\mu_0). \end{aligned} \quad (40)$$

and the NLO functions $A_1(y_t)$ and $A_1(y_{t'})$ by

$$A_1(y_i) = -2 \delta C_7^{(1)}(\mu_0), \quad F_1(y_i) = -2 \delta C_8^{(1)}(\mu_0). \quad (41)$$

The NLO contributions to the Wilson coefficients (in our 4G2HDMs) are given by^[3]

$$\delta C_i^{(1)eff}(\mu_0) = 0 \quad i = 1, 2, 3, 5, 6 \quad (42)$$

$$E_0(y_i) = \delta C_4^{(1)}(\mu_0) = A_{U_i} \left[\frac{3y_i^2 - 2y_i}{6(1-y_i)^4} \ln y_i + \frac{-7y_i^3 + 29y_i^2 - 16y_i}{36(1-y_i)^3} \right], \quad (43)$$

and

$$\begin{aligned} \delta C_7^{(1)}(\mu_0) &= A_{U_i} \left\{ \frac{16y_i^4 - 74y_i^3 + 36y_i^2}{9(1-y_i)^4} Li_2 \left(1 - \frac{1}{y_i} \right) + \frac{-63y_i^4 + 807y_i^3 - 463y_i^2 + 7y_i}{81(1-y_i)^5} \ln y_i \right. \\ &+ \frac{-1202y_i^4 + 7569y_i^3 - 5436y_i^2 + 797y_i}{486(1-y_i)^4} + \left[\frac{6y_i^4 + 46y_i^3 - 28y_i^2}{9(1-y_i)^5} \ln y_i \right. \\ &+ \left. \left. \frac{-14y_i^4 + 135y_i^3 - 18y_i^2 - 31y_i}{27(1-y_i)^4} \right] \ln \frac{\mu_0^2}{m_i^2} \right\} + A_{D_i} \left\{ \frac{-32y_i^3 + 112y_i^2 - 48y_i}{9(1-y_i)^3} Li_2 \left(1 - \frac{1}{y_i} \right) \right. \\ &+ \frac{14y_i^3 - 128y_i^2 + 66y_i}{9(1-y_i)^4} \ln y_i + \frac{8y_i^3 - 52y_i^2 + 28y_i}{3(1-y_i)^3} + \left[\frac{-12y_i^3 - 56y_i^2 + 32y_i}{9(1-y_i)^4} \ln y_i \right. \\ &+ \left. \left. \frac{16y_i^3 - 94y_i^2 + 42y_i}{9(1-y_i)^3} \right] \ln \frac{\mu_0^2}{m_i^2} \right\}, \end{aligned} \quad (44)$$

$$\begin{aligned} \delta C_8^{(1)}(\mu_0) &= A_{U_i} \left\{ \frac{13y_i^4 - 17y_i^3 + 30y_i^2}{6(1-y_i)^4} Li_2 \left(1 - \frac{1}{y_i} \right) + \frac{-468y_i^4 + 321y_i^3 - 2155y_i^2 - 2y_i}{216(1-y_i)^5} \ln y_i \right. \\ &+ \frac{-4451y_i^4 + 7650y_i^3 - 18153y_i^2 + 1130y_i}{1296(1-y_i)^4} + \left[\frac{-17y_i^3 - 31y_i^2}{6(1-y_i)^5} \ln y_i \right. \\ &+ \left. \left. \frac{-7y_i^4 + 18y_i^3 - 261y_i^2 - 38y_i}{36(1-y_i)^4} \right] \ln \frac{\mu_0^2}{m_i^2} \right\} + A_{D_i} \left\{ \frac{-17y_i^3 + 25y_i^2 - 36y_i}{6(1-y_i)^3} Li_2 \left(1 - \frac{1}{y_i} \right) \right. \\ &+ \frac{34y_i^3 - 7y_i^2 + 165y_i}{12(1-y_i)^4} \ln y_i + \frac{29y_i^3 - 44y_i^2 + 143y_i}{8(1-y_i)^3} + \left[\frac{17y_i^2 + 19y_i}{3(1-y_i)^4} \ln y_i \right. \\ &+ \left. \left. \frac{7y_i^3 - 16y_i^2 + 81y_i}{6(1-y_i)^3} \right] \ln \frac{\mu_0^2}{m_i^2} \right\}. \end{aligned} \quad (45)$$

The electroweak and non-perturbative corrections are retained to their SM predictions as given in [69] (see also eq. 26), i.e., we do not take into account the effect of our 4G2HDM on these corrections.

[3] The NLO results for the Wilson coefficients in a 2HDM can be found in [51, 71].

2. $B_q - \bar{B}_q$ mixing

In the SM, $B_q - \bar{B}_q$ mixing ($q = d, s$) proceeds to an excellent approximation only through the box diagrams with internal top quark exchanges. On the other hand, in our 4G2HDMs there are additional contributions to $B_q - \bar{B}_q$ mixing coming from the loop exchanges of the t' and charged-Higgs.

In the 4G2HDM, the mass difference $\Delta M_q = 2|M_{12_q}|$ is given at LO by^[4]

$$M_{12_q} = \frac{G_F^2}{12\pi^2} M_W^2 f_{B_q}^2 B_q M_{B_q} [M_{WW} + M_{HH} + M_{HW}], \quad (46)$$

where we have used

$$\langle B_q | (\bar{s}b)_{(V-A)} (\bar{s}b)_{(V-A)} | B_q \rangle = \frac{8}{3} f_{B_q}^2 B_q M_{B_q}^2, \quad (47)$$

$$\langle B_q | (\bar{s}b)_{(S+P)} (\bar{s}b)_{(S+P)} | B_q \rangle = -\frac{5}{3} f_{B_q}^2 B_q M_{B_q}^2. \quad (48)$$

and

$$\begin{aligned} M_{WW} &= \lambda_{bq}^t{}^2 \eta_{tt} S_{WW}(x_t) + \lambda_{bq}^{t'}{}^2 \eta_{t't'} S_{WW}(x_{t'}) + 2 \lambda_{bq}^t \lambda_{bq}^{t'} \eta_{tt'} S_{WW}(x_t, x_{t'}), \\ M_{HH} &= \lambda_{bq}^t{}^2 S_{HH}(y_t) + \lambda_{bq}^{t'}{}^2 S_{HH}(y_{t'}) + 2 \lambda_{bq}^t \lambda_{bq}^{t'} S_{HH}(y_t, y_{t'}), \\ M_{HW} &= \lambda_{bq}^t{}^2 S_{HW}(x_t, z) + \lambda_{bq}^{t'}{}^2 S_{HW}(x_{t'}, z) + 2 \lambda_{bq}^t \lambda_{bq}^{t'} S_{HW}(x_t, x_{t'}, z), \end{aligned} \quad (49)$$

with $z = \frac{m_{H^+}^2}{m_W^2}$, $x_i = \frac{m_i^2}{m_W^2}$, $y_i = \frac{m_i^2}{m_{H^+}^2}$ ($i = t$ or t') and $\lambda_{d_i d_j}^u \equiv V_{ud_i}^* V_{ud_j}$.

The contributions from W -exchange diagrams with q_i and q_j (i, j are generation indices) as the internal quarks are given by,

$$S_{WW}(x_i, x_j) = x_i x_j \left\{ \left[\frac{1}{4} + \frac{3}{2} \frac{1}{(1-x_j)} - \frac{3}{4} \frac{1}{(1-x_j)^2} \right] \frac{\ln x_j}{(x_j - x_i)} + (x_j \rightarrow x_i) - \frac{3}{4} \frac{1}{(1-x_i)(1-x_j)} \right\}, \quad (50)$$

and $S_{WW}(x_i) \equiv S_{WW}(x_i, x_i)$ can be obtained from Eq. 50 by taking the limit $x_j \rightarrow x_i$.

The contributions from the H^+ -exchange diagrams are given by

$$\begin{aligned} S_{HH}(y_t, y_{t'}) &= z S_{L_1} S_{L_2} \left[\frac{S_{HH}^{k2}(y_t, y_{t'})}{4} B_{L_1} B_{L_2} - \frac{5}{8} x_b S_{HH}^m(y_t, y_{t'}) B_{R_1} B_{R_2} \right], \\ S_{HH}(y_t) &= z S_{L_2}^2 \left[\frac{S_{HH}^{k2}(y_t)}{4} B_{L_2}^2 - \frac{5}{8} x_b S_{HH}^m(y_t) B_{R_2}^2 \right], \\ S_{HH}(y_{t'}) &= z S_{L_1}^2 \left[\frac{S_{HH}^{k2}(y_{t'})}{4} B_{L_1}^2 - \frac{5}{8} x_b S_{HH}^m(y_{t'}) B_{R_1}^2 \right], \end{aligned} \quad (51)$$

where $x_b = \frac{m_b^2}{m_{H^+}^2} \frac{M_{B_q}^2}{m_b(m_b)^2}$,

$$S_{HH}^{k2}(y_i, y_j) = y_i y_j \left\{ \frac{1}{(y_i - y_j)} \left(\frac{y_i^2 \ln y_i}{(1-y_i)^2} - \frac{y_j^2 \ln y_j}{(1-y_j)^2} \right) + \frac{1}{(1-y_i)(1-y_j)} \right\}, \quad (52)$$

$$S_{HH}^{k2}(y_i) = S_{HH}^{k2}(y_i, y_j)_{y_j \rightarrow y_i}, \quad (53)$$

$$S_{HH}^m(y_i, y_j) = y_i y_j \left\{ \frac{1}{(y_i - y_j)} \left(\frac{y_i \ln y_i}{(1-y_i)^2} - \frac{y_j \ln y_j}{(1-y_j)^2} \right) + \frac{1}{(1-y_i)(1-y_j)} \right\}, \quad (54)$$

$$S_{HH}^m(y_i) = S_{HH}^m(y_i, y_j)_{y_j \rightarrow y_i}. \quad (55)$$

[4] The LO results for $B_q - \bar{B}_q$ mixing in a “standard” 2HDM of type II with three generations of fermion doublets are given in [72].

and the terms

$$\begin{aligned}
B_{L_1} &= -A_{u_1} + A_{u_2} \Sigma_{t't'} + A_{u_2} \frac{m_t}{m_{t'}} \frac{V_{tb}}{V_{t'b}} \Sigma_{tt'}, \\
B_{L_2} &= -A_{u_1} + A_{u_2} \Sigma_{tt} + A_{u_2} \frac{m_{t'}}{m_t} \frac{V_{t'b}}{V_{tb}} \Sigma_{t't}, \\
S_{L_1} &= -A_{u_1} + A_{u_2} \Sigma_{t't'} + A_{u_2} \frac{m_t}{m_{t'}} \frac{V_{ts}^*}{V_{t's}^*} \Sigma_{tt'}, \\
S_{L_2} &= -A_{u_1} + A_{u_2} \Sigma_{tt} + A_{u_2} \frac{m_{t'}}{m_t} \frac{V_{ts}^*}{V_{t's}^*} \Sigma_{t't}, \\
B_{R_1} &= A_{d_1} - A_{d_2} \Sigma_{bb} - A_{d_2} \frac{m_{b'}}{m_b} \frac{V_{t'b'}}{V_{t'b}} \Sigma_{b'b}, \\
B_{R_2} &= A_{d_1} - A_{d_2} \Sigma_{bb} - A_{d_2} \frac{m_{b'}}{m_b} \frac{V_{tb'}}{V_{tb}} \Sigma_{b'b},
\end{aligned} \tag{56}$$

are obtained from the $b \rightarrow t, t'$ and $t, t' \rightarrow s$ vertices in the box diagrams.

The functions $S_{HW}(x_i, x_j, z)$ obtained from diagrams with both W and H^+ -exchanges are given by

$$S_{HW}(x_t, x_{t'}, z) = 2x_t x_{t'} (S_{L_1} B_{L_2} + S_{L_2} B_{L_1}) \left[\frac{S_1(x_t, x_{t'}, z)}{4} + S_2(x_t, x_{t'}, z) \right], \tag{57}$$

$$S_{HW}(x_t, z) = 2x_t^2 S_{L_2} B_{L_2} \left[\frac{S_1(x_t, z)}{4} + S_2(x_t, z) \right], \tag{58}$$

$$S_{HW}(x_{t'}, z) = 2x_{t'}^2 S_{L_1} B_{L_1} \left[\frac{S_1(x_{t'}, z)}{4} + S_2(x_{t'}, z) \right], \tag{59}$$

where

$$\begin{aligned}
S_1(x_i, x_j, z) &= \frac{z \ln z}{(1-z)(z-x_i)(z-x_j)} + \frac{x_i \ln x_i}{(1-x_i)(x_i-z)(x_i-x_j)} + \frac{x_j \ln x_j}{(1-x_j)(x_j-z)(x_j-x_i)}, \\
S_2(x_i, x_j, z) &= -\frac{z^2 \ln z}{(1-z)(z-x_i)(z-x_j)} - \frac{x_i^2 \ln x_i}{(1-x_i)(x_i-z)(x_i-x_j)} - \frac{x_j^2 \ln x_j}{(1-x_j)(x_j-z)(x_j-x_i)},
\end{aligned} \tag{60}$$

and the functions $S_1(x_i, z)$ and $S_2(x_i, z)$ can be derived from the expressions for $S_1(x_i, x_j, z)$ and $S_2(x_i, x_j, z)$, respectively, by taking the limit $x_j \rightarrow x_i$.

3. Combined constraints

Using the analysis above, we derive below the constraints on our 4G2HDMs that come from $Br(B \rightarrow X_s \gamma)$ and ΔM_q ($q = d, s$). For the B-physics parameters we use the inputs given in Table I. As an illustration, the 4th generation quark masses are fixed to $m_{t'} = 500$ GeV and $m_{b'} = 450$ GeV, consistent with the direct limits from the Tevatron [32] and the perturbative unitarity upper bounds [34, 73].^[5] We vary the charged Higgs mass in the range $200 \text{ GeV} < m_{H^+} < 1 \text{ TeV}$ and study the dependence on ϵ_t in the range $0 < \epsilon_t < 1$, while fixing $\epsilon_b = m_b/m_{b'} (\sim 0.01)$. We also vary the 4×4 CKM element $V_{t'b}$ in the range $0 < |V_{t'b}| < 0.2$ (see also next section), keeping $|\lambda_{sb}^{t'}| \leq 0.02$ and varying $\tan \beta$ in the range, $1 < \tan \beta < 30$. We made a scan over the entire parameter space by a flat random number generator and obtained bounds and correlations among the various parameters mentioned above.

Let us first consider the case $V_{t'b} \rightarrow 0$, corresponding to the “3+1” scenario, in which the 4th generation quarks do not mix with the quarks of the 1st three generations (we assume that $|V_{t'b}| \gg |V_{t's}|, |V_{t'd}|$). In this case, the top-quark loops become dominant, since contributions to the amplitudes of $B \rightarrow X_s \gamma$ and $B_q - \bar{B}_q$ mixing from t' -loops are mostly suppressed apart from the terms which are proportional to $(m_{b'}/m_b) \cdot \lambda_{bs}^{t'}$ (see Eqs. 36 and 56).

In Figs. 2, 3 and 4 we plot the allowed ranges in the $m_{H^+} - \tan \beta$ (left plots) and the $\tan \beta - \epsilon_t$ (right plots) planes, in the 4G2HDM of types I, II and III, respectively, using $|V_{t'b}| = 0.001$ (with $|\lambda_{sb}^{t'}| = 10^{-5}$ correspondingly).

[5] There is a very weak dependence of $B \rightarrow X_s \gamma$ and $B - \bar{B}$ -mixing on the b' -mass, since it enters only in the the $H^+ u d$ Yukawa couplings with no dynamical and/or kinematical dependence.

$f_{bd}\sqrt{B_{bd}} = 0.224 \pm 0.015 \text{ GeV} [74, 75]$ $\xi = 1.232 \pm 0.042 [74, 75]$ $\eta_t = 0.5765 \pm 0.0065 [76]$ $\Delta M_s = (17.77 \pm 0.12) ps^{-1}$ $\Delta M_d = (0.507 \pm 0.005) ps^{-1}$ $f_B = (0.208 \pm 0.008) \text{ GeV}$ $m_t^{pole} = (170 \pm 4) \text{ GeV}$	$ V_{ub} = (32.8 \pm 2.6) \times 10^{-4}^a$ $ V_{cb} = (40.86 \pm 1.0) \times 10^{-3}$ $\gamma = (73.0 \pm 13.0)^\circ$ $\mathcal{BR}(B \rightarrow X_s \gamma) = (3.55 \pm 0.25) \times 10^{-4}$ $m_b(m_b) = 4.23 \text{ GeV}$ $\alpha_s(M_Z) = 0.11$ $\tau_{B^+} = 1.63 ps$ $m_\tau = 1.77 \text{ GeV}$
---	--

^aIt is the weighted average of $V_{ub}^{ini} = (40.1 \pm 2.7 \pm 4.0) \times 10^{-4}$ and $V_{ub}^{exl} = (29.7 \pm 3.1) \times 10^{-4}$. In our numerical analysis, we increase the error on V_{ub} by 50% and take the total error to be around 12% due to the appreciable disagreement between the two determinations.

TABLE I: Inputs used in order to constrain the 4G2HDM parameter space. When not explicitly stated, we take the inputs from Particle Data Group [49].

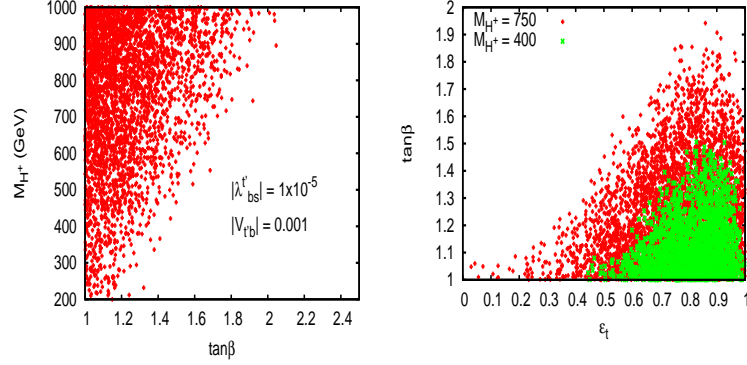


FIG. 2: The allowed parameter space in the $m_{H^+} - \tan \beta$ and $\tan \beta - \epsilon_t$ planes, following constraints from $B \rightarrow X_s \gamma$ and $B_q - \bar{B}_q$ mixing, in the 4G2HDM-I, for $V_{t'b} = 0.001$, $m_{t'} = 500 \text{ GeV}$, $m_{b'} = 450 \text{ GeV}$ and $\epsilon_b = m_b/m_{b'}$.

We see that in the type-I 4G2HDM, the “3+1” scenario typically imposes $\tan \beta \sim 1$ with ϵ_t typically larger than about 0.4 when $m_{H^+} \lesssim 500 \text{ GeV}$. In particular, for a fixed ϵ_t the upper bound on $\tan \beta$ is reduced with the charged Higgs mass, allowing $m_{H^+} \gtrsim 200 \text{ GeV}$ for $\tan \beta \sim 1$ and restricting $m_{H^+} \gtrsim 500 \text{ GeV}$ for $\tan \beta \gtrsim 1.5$. In the type II and type III 4G2HDMs we observe a similar correlation between $\tan \beta$ and m_{H^+} , however, larger $\tan \beta$ are allowed for $\epsilon_t \lesssim m_t/m_{t'}$ and a charged Higgs mass typically heavier than 400 GeV.

Let us now turn to the case of a Cabibbo size mixing between the 4th and 3rd generation quarks, setting $|V_{t'b}| = |V_{tb'}| = 0.2$. In Fig. 5 we show the allowed parameter space in the $\tan \beta - \epsilon_t$ plane in the 4G2HDM-I, II and III with $|V_{t'b}| = 0.2$, $m_{t'} = 500 \text{ GeV}$, $m_{b'} = 450 \text{ GeV}$ and $\epsilon_b = m_b/m_{b'}$. In addition, we take $|\lambda_{sb}^t| = 0.004$ for Type-I and 0.001 for Type-II and III models and depict these correlations for two different values of the charged Higgs mass: $M_{H^+} = 400$ and 750 GeV. In the type II and type III 4G2HDMs we see a similar behavior as in the no mixing case ($V_{t'b} \rightarrow 0$), while in the 4G2HDM-I we see that “turning on” $V_{t'b}$ allows for a slightly larger $\tan \beta$, i.e., up to $\tan \beta \sim 5$

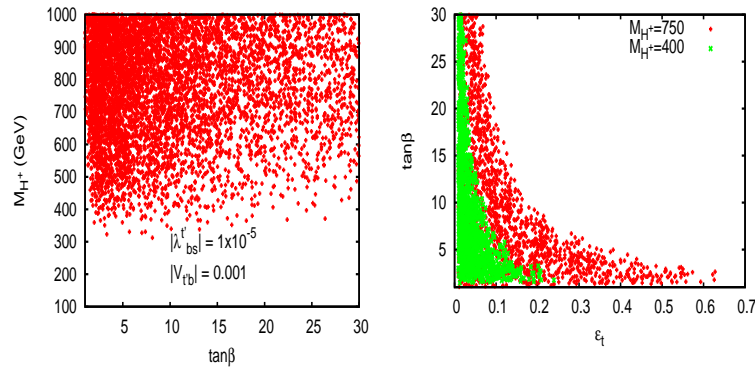


FIG. 3: Same as Fig. 2 for the 4G2HDM-II.

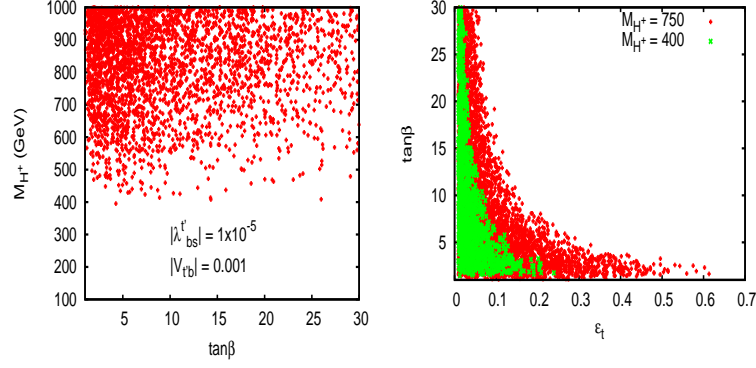


FIG. 4: Same as Fig. 2 for the 4G2HDM-III.

for $\epsilon_t \gtrsim 0.9$.

With a similar set of inputs, setting now $\epsilon_t \sim m_t/m_{t'}$, in Figs. 6 and 7 we plot $\tan\beta$ as a function of M_{H^+} (where $|\lambda_{sb}^{t'}|$ is kept free) and of $\lambda_{sb}^{t'}$ (where M_{H^+} is kept free), respectively, in the three different types of our 4G2HDMs. We note that, similar to the no mixing case, larger values of $\tan\beta$ are allowed in the 4G2HDM of types II and III. Furthermore, $m_{H^+} \sim 300$ GeV and $\tan\beta \sim 1$ are allowed in the 4G2HDM-I, and from Fig. 6 we see that $|\lambda_{sb}^{t'}|$ up to 0.01 is allowed in the case of the 4G2HDM-I and II, while in 4G2HDM-III $|\lambda_{sb}^{t'}| \lesssim 0.005$ is typically required.

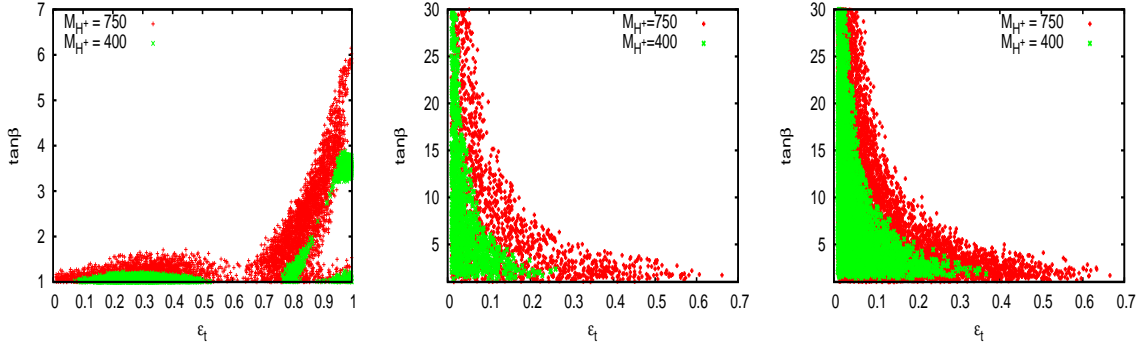


FIG. 5: Allowed parameter space in the $\tan\beta - \epsilon_t$ plane in the 4G2HDM of type-I (left), type-II (middle) and type-III (right), for $|V_{t'b}| = 0.2$, $m_{t'} = 500$ GeV, $m_{b'} = 450$ GeV, $\epsilon_b = m_b/m_{b'}$, $|\lambda_{sb}^{t'}| = 0.004$ and with $m_{H^+} = 400$ and 750 GeV.

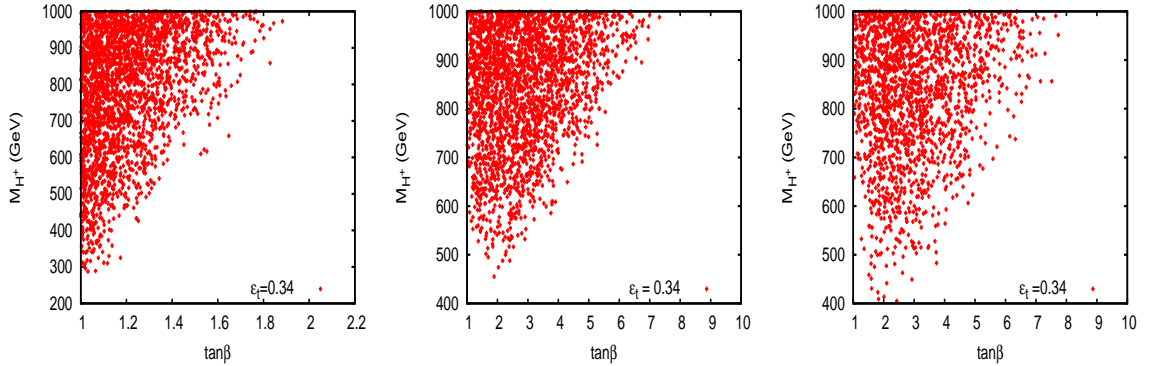


FIG. 6: Allowed parameter space in the $m_{H^+} - \tan\beta$ plane in the 4G2HDM of type-I (left), type-II (middle) and type-III (right), for $|V_{t'b}| = 0.2$, $m_{t'} = 500$ GeV, $m_{b'} = 450$ GeV, $\epsilon_b = m_b/m_{b'}$, $|\lambda_{sb}^{t'}| = 0.004$ and $\epsilon_t = 0.34 (\sim m_t/m_{t'})$.

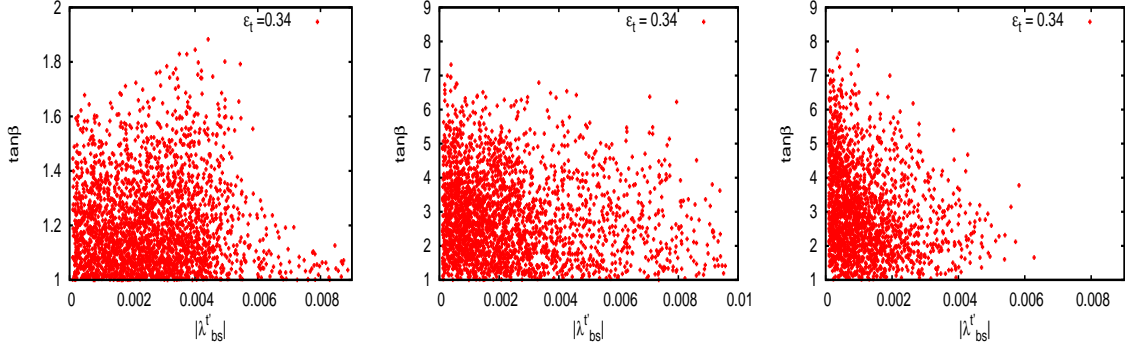


FIG. 7: Allowed parameter space in the $\tan\beta - |\lambda_{sb}^{t'}|$ plane in the 4G2HDM of type-I (left), type-II (middle) and type-III (right), for a fixed $|V_{t'b}| = 0.2$, $\epsilon_t \sim m_t/m_{t'}$ and for $m_{t'} = 500$ GeV, $m_{b'} = 450$ GeV and $\epsilon_b = m_b/m_{b'}$.

To summarize this section, we find that the parameter space of our 4G2HDMs, when subject to constraints from $Br(B \rightarrow X_s \gamma)$ and $B_q - \bar{B}_q$ mixing, can be characterized by the following features:

- In the type II and III 4G2HDMs large $\tan\beta \gtrsim 20$ are allowed for $\epsilon_t \lesssim 0.1$.
- In the 4G2HDM-I $\tan\beta$ is typically restricted to be $\tan\beta \sim \mathcal{O}(1)$ with $\epsilon_t \sim m_t/m_{t'}$, reaching at most $\tan\beta \sim 5$ if $\epsilon_t \sim 1$ and $V_{t'b} \sim \mathcal{O}(0.1)$, i.e., of the size of the Cabbibo angle.
- The charged Higgs mass is typically heavier than about 400 GeV in the type II and III 4G2HDM and is allowed to be as light as 200-300 GeV (depending on $V_{t'b}$) in the 4G2HDM-I. In all three models the lower bound on m_{H^+} increases (typically linearly) with $\tan\beta$; reaching $m_{H^+} \sim 1$ TeV already for $\tan\beta \sim 2$ in the 4G2HDM-I and $\tan\beta \sim 7$ in the type II and III 4G2HDMs if $\epsilon_t \sim m_t/m_{t'}$.
- In the 4G2HDM-III, $|\lambda_{sb}^{t'}| \lesssim 0.005$ is required if $\epsilon_t \sim m_t/m_{t'}$, but values up to $|\lambda_{sb}^{t'}| \sim 0.01$ are still allowed in the 4G2HDMs of types I and II.

B. Constraints from $Z \rightarrow b\bar{b}$

It has been long known that the decay $Z \rightarrow b\bar{b}$ is very sensitive to effects of new heavy particles, in particular, to the dynamics of multi-Higgs models through loop exchanges of both neutral and charged Higgs particles (see e.g., [77, 78]). The $Zb\bar{b}$ vertex can be parameterized as follows:

$$V_{qqZ} \equiv -i \frac{g}{c_W} \bar{q} \gamma_\mu (\bar{g}_{qL} L + \bar{g}_{qR} R) q Z^\mu, \quad (61)$$

where $s_W(c_W) = \sin\theta_W(\cos\theta_W)$, $L(R) = (1 - (+)\gamma_5)/2$ and

$$\bar{g}_{qL,R} = g_{qL,R}^{SM} + g_{qL,R}^{new}, \quad (62)$$

so that $g_{qL,R}^{SM}$ are the SM (1-loop) quantities and $g_{qL,R}^{new}$ are the new physics 1-loop corrections.

The effects of the new physics, $g_{qL,R}^{new}$, is best studied via the well measured quantity R_b :

$$R_b \equiv \frac{\Gamma(Z \rightarrow b\bar{b})}{\Gamma(Z \rightarrow \text{hadrons})}, \quad (63)$$

which is a rather clean test of the SM. In particular, being a ratio between two hadronic rates, most of the electroweak, oblique and QCD corrections cancel between numerator and denominator.

Following the analysis in [77], we parameterize the effects of new physics in R_b in terms of the corrections δ_b and δ_c to the decays $Z \rightarrow b\bar{b}$ and $Z \rightarrow c\bar{c}$, respectively:

$$R_b = R_b^{SM} \frac{1 + \delta_b}{1 + R_b^{SM} \delta_b + R_c^{SM} \delta_c}, \quad (64)$$

where $R_b^{SM} = 0.21578 \pm 0.00005$ and $R_c^{SM} = 0.17224 \pm 0.00003$ [79] are the corresponding 1-loop quantities calculated in the SM, and δ_q are the new physics corrections defined in terms of the $Zq\bar{q}$ couplings as:

$$\delta_q = 2 \frac{g_{qL}^{SM} g_{qL}^{new} + g_{qR}^{SM} g_{qR}^{new}}{(g_{qL}^{SM})^2 + (g_{qR}^{SM})^2}, \quad (65)$$

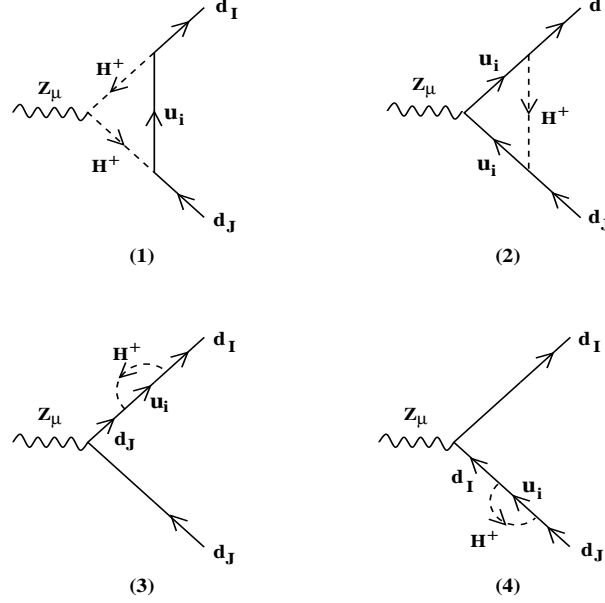


FIG. 8: One-loop diagrams for corrections to $Z \rightarrow d_I \bar{d}_J$ from charged Higgs loops.

With the new scalar-fermion interactions in Eqs. 4-7, the corrections to R_b from a 4th generation quarks in our 4G2HDMs are of three types: (i) the SM4-like corrections due to the 1-loop $W - t'$ exchanges (see also [17, 80, 81]), (ii) the 1-loop diagrams in Fig. 8 involving the $H^+ - t'$ exchanges and (iii) the 1-loop corrections involving the FC $\mathcal{H}^0 b\bar{b}'$ interactions (coming from the non-diagonal 34 and 43 elements in Σ^d), where $\mathcal{H}^0 = h, H$ or A .

Let us first consider the SM4-like (non-decoupling) correction to R_b , i.e., g_{qL}^{SM4} from the 1-loop diagrams involving the $W - t'$ exchanges (which are also present in our 4G2HDMs). It is given by [17, 80]:

$$g_{qL}^{SM4} = \frac{g^2}{64\pi^2 c_W^2} \left(\frac{m_{t'}^2}{m_Z^2} - \frac{m_t^2}{m_Z^2} \right) \sin^2 \theta_{34}, \quad (66)$$

where θ_{34} is the mixing angle between the 3rd and 4th generation quarks, i.e., defining $|V_{t'b}| = |V_{tb'}| \equiv \sin \theta_{34}$. This SM4-like effect on R_b is plotted in Fig. 9. We see that R_b puts rather stringent constraints on the $m_{t'} - \theta_{34}$ plane which is the SM4 subspace of the parameter space of our 4G2HDMs. In particular, increasing the t' mass would tighten the constraints on θ_{34} ; e.g., for $m_{t'} \sim 500$ GeV the $t' - b$ mixing angle is restricted to $\theta_{34} \lesssim 0.2$. The upper bound on θ_{34} stays roughly the same in our 4G2HDMs where the effects from the charged Higgs loops are included. For concreteness, for the rest of this section we will fix θ_{34} to either $\theta_{34} = 0$ or $\theta_{34} = 0.1, 0.2$, representing the no-mixing or mixing cases.

Using the generic formula given in [82], we calculated the 1-loop corrections to R_b from the charged-Higgs and from the FC neutral-Higgs exchanges and found that:

- In all three models, i.e., 4G2HDM-I,II,III, $\delta_c \ll \delta_b$, so that we can safely neglect the new effects in $Z \rightarrow c\bar{c}$.
- The 1-loop FC neutral-Higgs contributions are much smaller than the 1-loop charged-Higgs contributions shown in Fig. 8, in particular for $\epsilon_b \ll 1$. We, therefore, focus below only on the leading effects coming from the charged-Higgs sector.

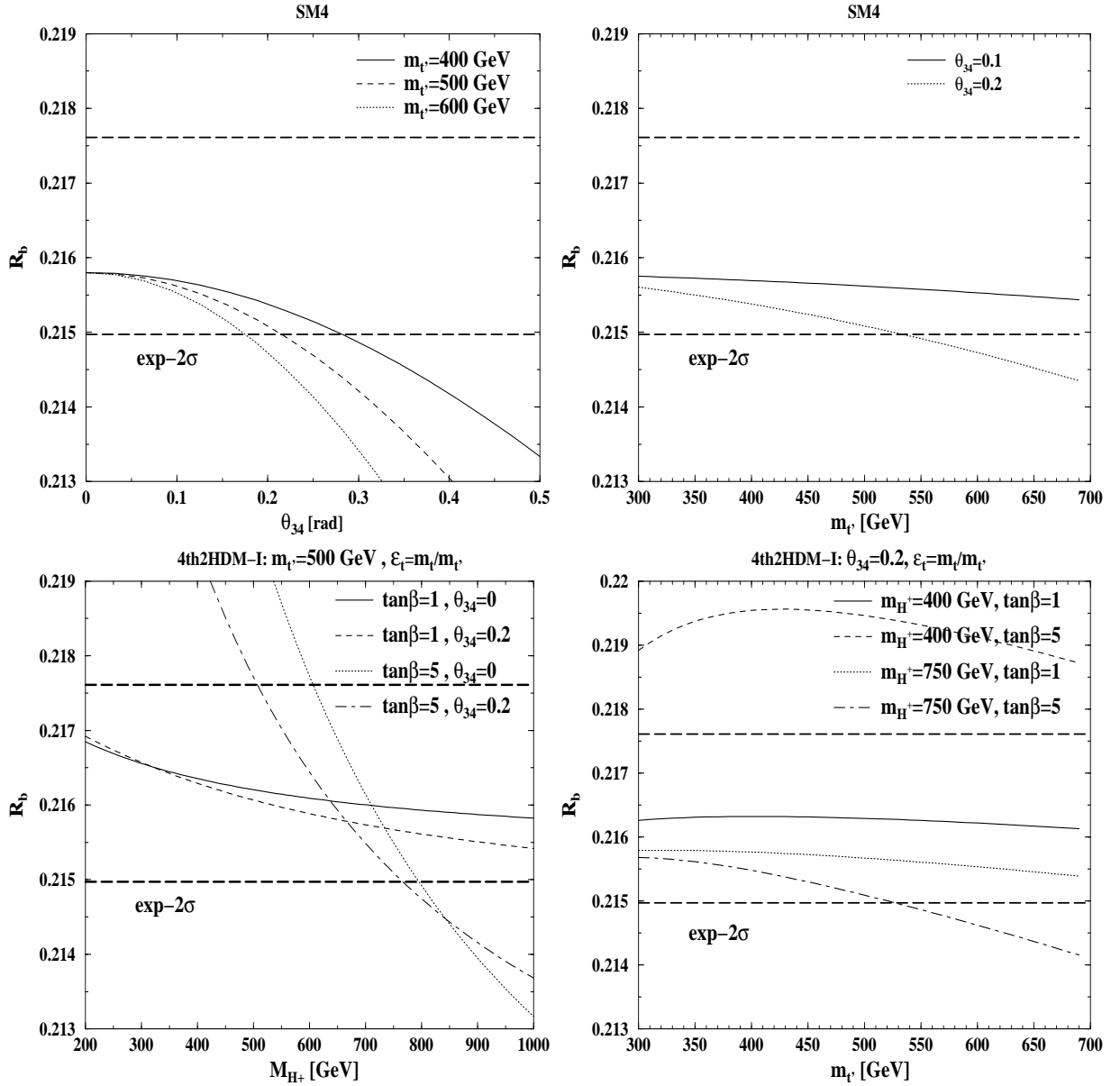


FIG. 9: Upper plots: R_b in the SM4, as a function of θ_{34} for several values of the t' mass (left) and as a function of $m_{t'}$ for $\theta_{34} = 0.1$ and 0.2 (right). Lower plots: R_b in the 4G2HDM-I, as a function of the charged Higgs mass for $m_{t'} = 500$ GeV, $\epsilon_t = m_t/m_{t'}$ and for $(\tan\beta, \theta_{34}) = (1, 0), (1, 0.2), (5, 0), (5, 0.2)$ (left), and as a function of $m_{t'}$ for $\theta_{34} = 0.2$, $\epsilon_t = m_t/m_{t'}$ and for $(m_{H+} [\text{GeV}], \tan\beta) = (400, 1), (400, 5), (750, 1), (750, 5)$ (right).

- The charged-Higgs interactions in models 4G2HDM-II and 4G2HDM-III have negligible effects on R_b and are, therefore, not constrained by this quantity. On the other hand, R_b is rather sensitive to the charged Higgs loop exchanges within our type I 4G2HDM.

In light of the above findings, we plot in Fig. 9 the quantity R_b in the 4G2HDM-I (calculated from Eq. 64), as a function of the charged Higgs and t' masses, fixing $\epsilon_t = m_t/m_{t'}$ and focusing on the values $\tan\beta = 1, 5$, $\theta_{34} = 0, 0.2$ and $m_{H+} = 400, 750$ GeV. We see that, while there are no constraints from R_b on the charged Higgs and t' masses if $\tan\beta = 1$, for higher values of $\tan\beta$ a more restricted region of the charged Higgs mass is allowed which again depends on θ_{34} , e.g., for $\tan\beta = 5$, $550 \text{ GeV} \lesssim m_{H+} \lesssim 800 \text{ GeV}$, and $m_{t'} \lesssim 500 \text{ GeV}$ is required in order for R_b to be within its 2σ measured value ($R_b^{\text{exp}} = 0.21629 \pm 0.00066$ [79]).

In Fig. 10 we show the allowed ranges in the $m_{H+} - \tan\beta$ plane in the 4G2HDM-I, subject to the R_b constraint

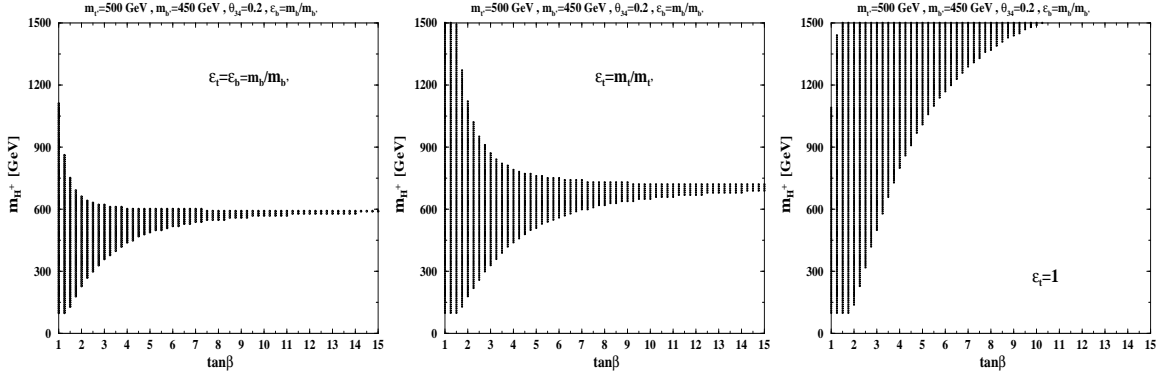


FIG. 10: Allowed area in the $m_{H^+} - \tan\beta$ in the 4G2HDM-I, subject to the R_b measurement (within 2σ), for $m_{t'} = 500$ GeV, $m_{b'} = 450$ GeV, $\theta_{34} = 0.2$, $\epsilon_b = m_b/m_{b'}$ and for three values of the $t - t'$ mixing parameter: $\epsilon_t = \epsilon_b \sim 0.01$ (left plot), $\epsilon_t = m_t/m_{t'} \sim 0.35$ (middle plot) and $\epsilon_t = 1$ (right plot).

(2σ), for $\tan\beta$ in the range 1-15, fixing $m_{t'} = 500$ GeV, $m_{b'} = 450$ GeV, $\theta_{34} = 0.2$, $\epsilon_b = m_b/m_{b'}$ (which also enters the $t'bH^+$ vertex) and for three representative values of the $t - t'$ mixing parameter: $\epsilon_t = \epsilon_b \sim 0.01$, $\epsilon_t = m_t/m_{t'} \sim 0.35$ and $\epsilon_t = 1$. As expected, when $\tan\beta$ is lowered, the constraints on the charged Higgs mass are weakened. We see e.g., that for $\epsilon_t = m_t/m_{t'} \sim 0.35$, $\tan\beta \sim 1$ is compatible with m_{H^+} values ranging from 200 GeV up to the TeV scale, while for $\tan\beta \sim 5$ the charged Higgs mass is restricted to be within the range $450 \text{ GeV} \lesssim m_{H^+} \lesssim 750 \text{ GeV}$. Note however, that in the 4G2HDM-I, $\tan\beta = 5$ with $\epsilon_t = m_t/m_{t'}$ is not allowed by constraints from B-physics flavor data (see previous section).

C. Constraints from the Oblique parameters

The sensitivity of 4th generation fermions to PEWD within the minimal SM4 framework was extensively analyzed in the past decade [49, 80, 83–87]. One of the immediate interesting consequences of the presence of the 4th generation fermion doublet (with respect to the PEWD constraints) is that it allows for a considerably heavier Higgs, thus removing the slight tension between the LEP II bound on the mass of the SM Higgs $m_H \gtrsim 115$ GeV and the corresponding theoretical best fitted value (to PEWD) $m_H = 87^{+35}_{-26}$ GeV [49]. In fact, a Higgs with $m_H \gtrsim 300$ GeV becomes favored in the SM4 when $m_{t'} - m_{b'} \sim 50$ GeV and θ_{34} is of the size of the Cabbibo angle, see e.g., [80, 85]. On the other hand, if, as in our case, the 4th generation fermions are embedded in a 2HDM framework, then there is a wider range of parameter space for which a lighter Higgs with a mass of $\mathcal{O}(100)$ GeV is allowed (see [36] and our analysis below). In addition, in the 2HDM case, the LEP II lower bound $m_H \gtrsim 115$ GeV can be relaxed, depending on the value of $\sin(\alpha - \beta)$ [$\sin(\alpha - \beta) = 1$ corresponds to the current SM bound] which controls the ZZH coupling responsible for the Higgs production mechanism at LEP.

In general, the contributions to the oblique parameters (S, T, U) of 4th generation fermions ($\Delta S_f, \Delta T_f, \Delta U_f$) and of extra scalars ($\Delta S_s, \Delta T_s, \Delta U_s$) are calculated with respect to the SM values and are bounded by a fit to PEWD [88]:

$$\begin{aligned} \Delta S &= S - S_{SM} = 0.02 \pm 0.11 \\ \Delta T &= T - T_{SM} = 0.05 \pm 0.12 \\ \Delta U &= U - U_{SM} = 0.07 \pm 0.12, \end{aligned} \quad (67)$$

where, following the fit made in [88], the SM values are defined for a Higgs mass reference value of $M_h^{ref} = 120$ GeV and for $m_t = 173.2$ GeV. The effects of our models (and in general of any heavy new physics) on the parameter U can be neglected. We, therefore, consider below the constraints from the 2-dimensional ellipse in the $S - T$ plane which, for a given confidence level (CL), is defined by (see e.g., [23]):

$$\begin{pmatrix} S - S_{exp} \\ T - T_{exp} \end{pmatrix}^T \begin{pmatrix} \sigma_S^2 & \sigma_S \sigma_T \rho \\ \sigma_S \sigma_T \rho & \sigma_T^2 \end{pmatrix} \begin{pmatrix} S - S_{exp} \\ T - T_{exp} \end{pmatrix} = -2 \ln(1 - CL), \quad (68)$$

where $S_{exp} = 0.02$ and $T_{exp} = 0.05$ are the best fitted (central) values in Eq. 67, $\sigma_S = 0.11, \sigma_T = 0.12$ are the corresponding standard deviations and $\rho = 0.879$ [88] is the (strong) correlation factor between S and T.

Note that the contribution of the Higgs spectrum of our 4G2HDMs to S and T are identical to that of any general 2HDM. We thus use the analytical expressions given in [83], where we also include in ΔT_f the new contributions from the $Wt'b$ and Wtb' off-diagonal CKM mixing angles (see e.g., [80]):

$$\Delta T_f = \frac{3}{8\pi s_W^2 c_W^2} \left(|V_{t'b'}|^2 F_{t'b'} + |V_{t'b}|^2 F_{t'b} + |V_{tb'}|^2 F_{tb'} - |V_{tb}|^2 F_{tb} + \frac{1}{3} F_{\ell_4 \nu_4} \right), \quad (69)$$

with

$$F_{ij} = \frac{x_i + x_j}{2} - \frac{x_i x_j}{x_i - x_j} \log \frac{x_i}{x_j}, \quad (70)$$

and $x_k \equiv (m_k/m_Z)^2$.

We first “blindly” (randomly) scan our parameter space, varying them in the ranges: $\tan\beta \leq 30$, $\theta_{34} \leq 0.3$, $100 \text{ GeV} \leq m_h \leq 1 \text{ TeV}$, $m_h \leq m_H \leq 1.5 \text{ TeV}$, $100 \text{ GeV} \leq m_A \leq 1 \text{ TeV}$, $400 \text{ GeV} \leq m_{t'}, m_{b'} \leq 600 \text{ GeV}$, $100 \text{ GeV} \leq m_{\nu'}, m_{\tau'} \leq 1.2 \text{ TeV}$,^[6] and the CP-even neutral Higgs mixing angle in the range $0 \leq \alpha \leq 2\pi$.

We use a sample of 100000 models (i.e., points in parameter space varied in the above specified ranges) and plot the result in Fig. 11. We find that out of the 100000 models about 3000 are within the 99%CL contour, 1500 within the 95%CL contour and 100 within the 68%CL contour. We compare these results to the SM4 case also shown in Fig. 11 (again using a sample of 100000 models), where the 4th generation quark and lepton masses as well as the (single) neutral Higgs mass are varied in the same ranges as specified above. We find that in the SM4 case only a few points (out of the 100000) are within the 68%CL S-T contour, while the number of SM4 points within the 95%CL and 99%CL allowed contours are comparable to the 2HDM case. This quantifies the slight preferability of the 2HDM (with respect to the amount of fine tuning required for compatibility with the available precision data) as an underlying framework for a 4th generation model.

We also examined the correlation in the $m_{H^+} - \tan\beta$ plane, when subject to the PEWD S-T constraint. This is shown in Fig. 12, where the data points are taken from the same 100000 sample used in Fig. 11 (i.e., the rest of the parameter space was varied in the ranges specified above). We see that compatibility with PEWD mostly requires $\tan\beta \sim \mathcal{O}(1)$ with a small number of points in parameter space having $\tan\beta \gtrsim 5$.

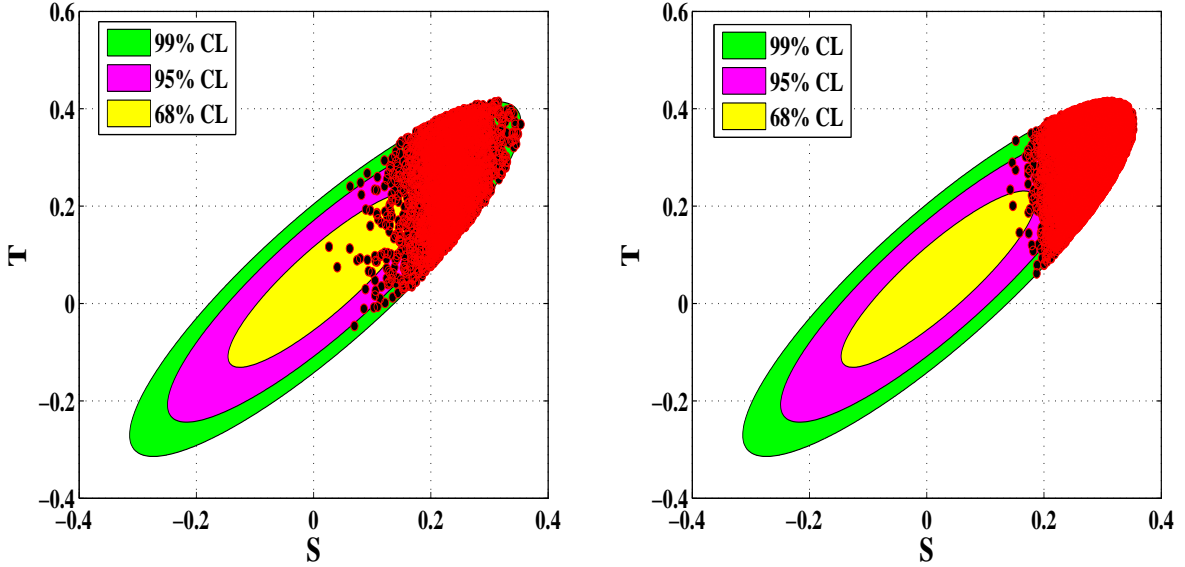


FIG. 11: The allowed points in parameter space projected onto the 68%, 95% and 99% allowed contours in the S - T plane, in the 4G2HDMs (left) and in the SM4 (right). The data points are varied in the ranges: $\tan\beta \leq 30$, $\theta_{34} \leq 0.3$, $100 \text{ GeV} \leq m_h \leq 1 \text{ TeV}$, $m_h \leq m_H \leq 1.5 \text{ TeV}$, $100 \text{ GeV} \leq m_A \leq 1 \text{ TeV}$, $400 \text{ GeV} \leq m_{t'}, m_{b'} \leq 600 \text{ GeV}$, $100 \text{ GeV} \leq m_{\nu'}, m_{\tau'} \leq 1.2 \text{ TeV}$ and the CP-even neutral Higgs mixing angle in the range $0 \lesssim \alpha \lesssim 2\pi$.

[6] Note that the perturbative unitarity upper bounds on the lepton masses are about twice larger than those on the quark masses [73]; thus allowing 4th generation lepton masses around 1 TeV.

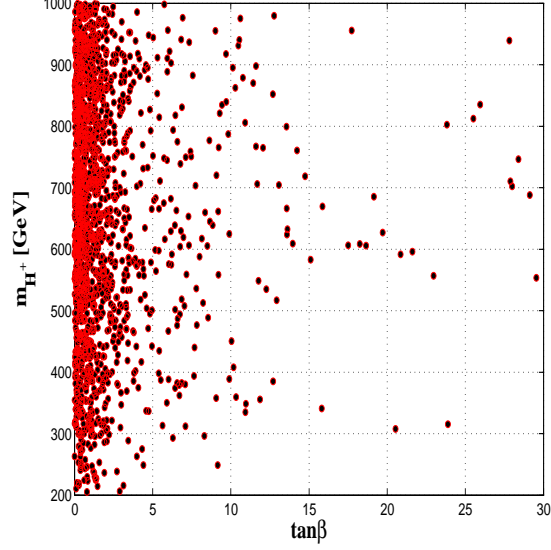


FIG. 12: 95% CL allowed range in the $m_{H^+} - \tan \beta$ plane. The data points are varied as specified in Fig. 11.

Next we consider the correlations between the mass splitting among the 4th generation quark masses, $\Delta m_{q'} \equiv m_{t'} - m_{b'}$, and the lepton masses $\Delta m_{\ell'} \equiv m_{\nu_4} - m_{\ell_4}$. In Fig. 13 we plot the 95%CL allowed regions (i.e., subject to the measured 95%CL contour in the S-T plane) for both the 4G2HDMs and the SM4 in the $\Delta m_{q'} - \Delta m_{\ell'}$ plane, again using the same data set of 100000 models used in Fig. 11. We see that, while in the SM4 case the allowed mass splittings are restricted to $-100 \text{ GeV} < \Delta m_{q'} < 100 \text{ GeV}$ and $-200 \text{ GeV} < \Delta m_{\ell'} < 200 \text{ GeV}$, in the 4G2HDMs these mass splitting ranges are significantly extended to: $-200 \text{ GeV} < \Delta m_{q'} < 200 \text{ GeV}$ and $-500 \text{ GeV} < \Delta m_{\ell'} < 400 \text{ GeV}$.

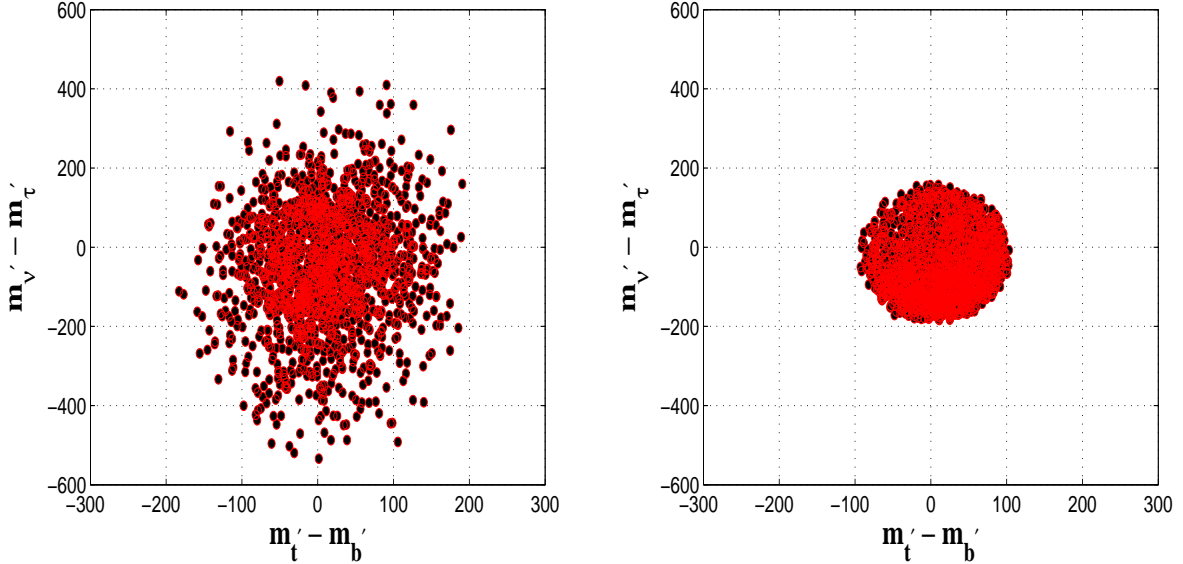


FIG. 13: Allowed regions in the $\Delta m_{q'} - \Delta m_{\ell'}$ plane within the 95%CL contour in the S-T plane, for the 4G2HDMs (left) and for the SM4 (right). The data points are varied as in Fig. 11.

In Figs. 14 we again plot the 95%CL allowed regions in the $\Delta m_{q'} - \Delta m_{\ell'}$ plane, for both the 4G2HDMs and the SM4, considering now the “3+1” scenario, i.e., with a vanishing mixing between the 4th generation quarks and the lighter three generations; $\theta_{34} = 0$. The rest of the parameter space is varied as in Fig. 13. We see that in the SM4

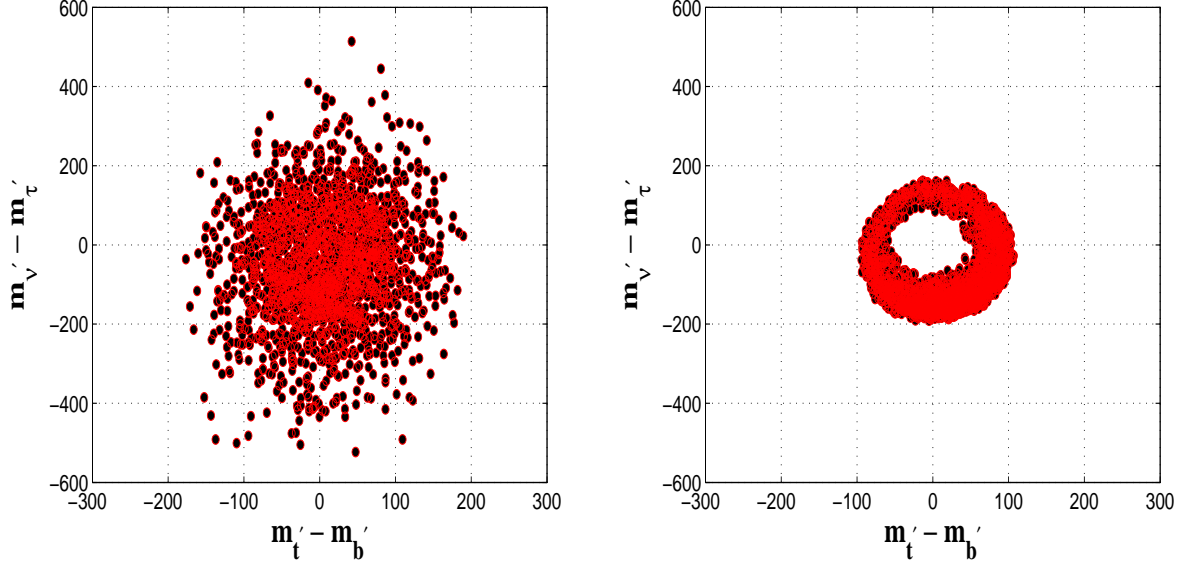


FIG. 14: Same as Fig. 13 but for $\theta_{34} = 0$; the rest of the parameter space is varied as in Fig. 13.

with $\theta_{34} \rightarrow 0$ there are no solutions where both the quark and lepton 4th generation doublets are degenerate, in particular, no solutions where both $|\Delta m_{q'}| \lesssim 50$ GeV and $|\Delta m_{\ell'}| \lesssim 100$ GeV. On the other hand, the implications of the no-mixing case on the 4G2HDMs are mild as there are still points/models for which the 4th generation quarks and leptons are both almost degenerate. For such small (or no) 4th generation fermion mass splitting the amount of isospin breaking required to compensate for the effect of the extra fermions and Higgs particles on S and T is provided by a mass splitting among the Higgs particles, as is shown below.

In order to demonstrate the interplay between the mass splittings in the Higgs and fermion sectors, we choose a more specific framework - partly motivated by our theoretical prejudice towards the possibility of dynamical EWSB, driven by the condensation(s) of the 4th generation fermions. In particular, we set $\alpha \sim \pi/2$, for which case $H \sim \text{Re}(\Phi_h^0)$ and $h \sim \text{Re}(\Phi_\ell)$; the heavier Higgs may be thus identified as a possible $\bar{Q}'Q'$ ($Q' = t', b'$) condensate, with a typical mass of $m_H \lesssim 2m_{Q'}$ [89]. We thus set $m_H = 1$ TeV and take a nearly degenerate 4th generation quark doublet with $m_{t'} = 500$ GeV and $m_{b'} = 490$ GeV. We further study two representative values for $\tan \beta$: $\tan \beta = 1$ and $\tan \beta = 5$, recalling that for $\tan \beta \sim \mathcal{O}(1)$, H^+ and A are roughly equal admixtures of Φ_ℓ and Φ_h , while if $\tan^2 \beta \gg 1$, one has $H^+ \sim \Phi_\ell^+$ and $A \sim \text{Im}(\Phi_h^0)$. The charged Higgs mass is set to $m_{H^+} = 600$ GeV, so that it is within the R_b constraints for both $\tan \beta = 1$ and $\tan \beta = 5$ when $\frac{m_b}{m_t} \lesssim \epsilon_t \lesssim \frac{m_t}{m_b}$ (see previous section). For simplicity we furthermore set $\theta_{34} = 0$ and vary the 4th generation lepton masses in the range $100 \text{ GeV} \lesssim m_{\nu'}, m_{\tau'} \lesssim 1.2 \text{ TeV}$ and the masses of the neutral Higgs particles, h and A , in the range $100 \text{ GeV} \lesssim m_h, m_A \lesssim 1000 \text{ GeV}$.

Using the above set of assumptions on our parameter space, we plot in Figs. 15 and 16 the 95%CL allowed region in the $\Delta m_{\ell'} - m_h$, the $m_h - m_A$ and the $\Delta m_{\ell'} - (m_h - m_A)$ planes, using again a sample of 100000 models with $\tan \beta = 1$ and $\tan \beta = 5$, respectively. Under the above set of inputs, we find the following noticeable features:

- There are allowed sets of points in parameter space (i.e., models) where both the 4th generation quarks and leptons are nearly degenerate with a mass splitting smaller than 50 GeV. These solutions require m_h and m_A to have a mass splitting smaller than about 400 GeV and to be within the narrow black bands in the $m_h - m_A$ plane, as seen in Figs. 15 and 16.
- There are allowed sets of points with a large splitting between the 4th generation leptons, $|m_{\nu'} - m_{\tau'}| > 300$ GeV. These cases require a large splitting also among m_h and m_A ; $400 \text{ GeV} \lesssim |m_h - m_A| \lesssim 800 \text{ GeV}$ if $\tan \beta = 1$ and $600 \text{ GeV} \lesssim |m_h - m_A| \lesssim 800 \text{ GeV}$ if $\tan \beta = 5$.
- For $\tan \beta = 1$, a splitting in the 4th generation lepton sector of $|m_{\nu'} - m_{\tau'}| > 200$ GeV requires m_h to be larger than about 400 GeV.

Finally, in Table II we give a list of interesting points (models) in parameter space (of our 4G2HDM of types I, II and III) that pass all the constraints considered in this chapter, i.e., from the S and T parameters, from R_b and from

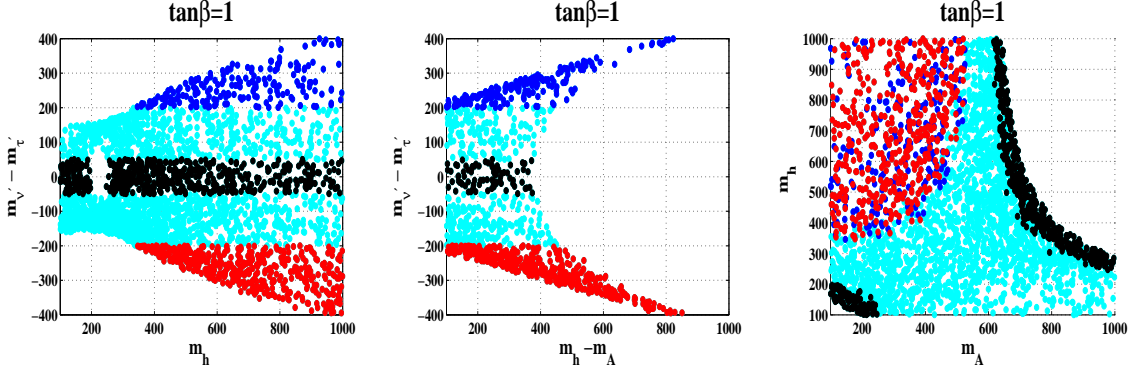


FIG. 15: 95% CL allowed regions in the $\Delta m_{\ell'} - m_h$ plane (left), in the $\Delta m_{\ell'} - (m_h - m_A)$ plane (middle) and in the $m_h - m_A$ plane (right), for $\tan\beta = 1$, $m_{H^+} = 600$ GeV, $\theta_{34} = 0$, $\alpha \sim \pi/2$, $m_{t'} = 500$ GeV and $m_{b'} = 490$ GeV. The lepton masses and Higgs masses are varied in the ranges: $100 \text{ GeV} \lesssim m_{\nu'}, m_{\tau'} \lesssim 1.2 \text{ TeV}$ and $100 \text{ GeV} \lesssim m_h, m_A \lesssim 1000 \text{ GeV}$. The black dots correspond to solutions with $|\Delta m_{\ell'}| < 50$ GeV, the red dot to solutions with $m_{\tau'} - m_{\nu'} > 200$ GeV and the blue dots to solutions with $m_{\nu'} - m_{\tau'} > 200$ GeV.

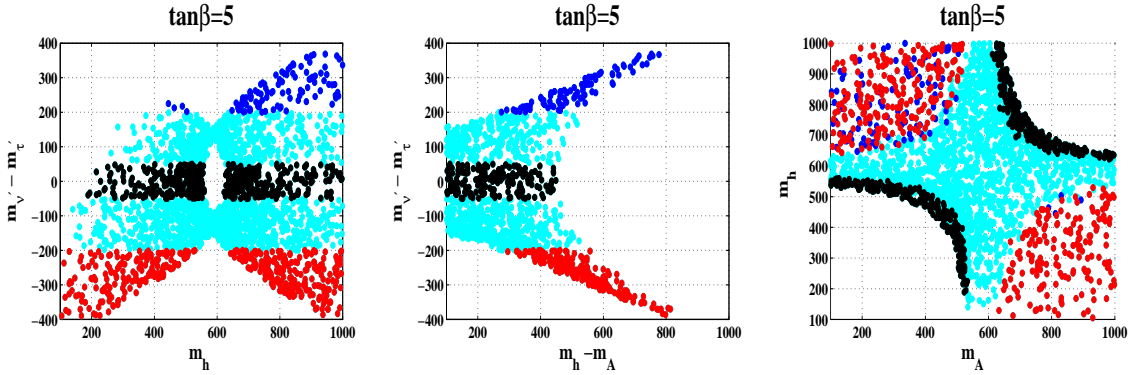


FIG. 16: Same as Fig. 15 for $\tan\beta = 5$.

B-physics flavor data. In particular, the list includes models with mass splittings between the up and down partners of both the 4th family quarks and leptons larger than 150 GeV, models with a light 100 – 200 GeV neutral Higgs, models with degenerate 4th generation doublets, models with a large inverted mass hierarchy in the quark doublet, i.e., $m_{b'} - m_{t'} > 150$ GeV, models with a light charged Higgs with a mass smaller than 500 GeV, models with a Cabbibo size as well as an $\mathcal{O}(0.01)$ size $t' - b/t - b'$ mixing angle (i.e., θ_{34}).

IV. PHENOMENOLOGY OF THE YUKAWA SECTOR IN THE 4G2HDM-I

Although this paper is not aimed to explore in detail the phenomenological consequences of the modifications to the Higgs Yukawa interactions involving the 4th generation quarks in our 4G2HDMs, in order to give a feel for their importance for collider searches of the 4th generation fermions, we consider below some phenomenological aspects of the 4G2HDM-I which is defined by $(\alpha_d, \beta_d, \alpha_u, \beta_u) = (0, 1, 0, 1)$. Recall that in this case, the Σ mixing matrices simplify to (keeping terms up to $\mathcal{O}(\epsilon_q^2)$, $q = b, t$):

$$\Sigma^d \simeq \begin{pmatrix} 0 & 0 & 0 & 0 \\ 0 & 0 & 0 & 0 \\ 0 & 0 & |\epsilon_b|^2 & \epsilon_b^* \\ 0 & 0 & \epsilon_b & \left(1 - \frac{|\epsilon_b|^2}{2}\right) \end{pmatrix}, \quad \Sigma^u \simeq \begin{pmatrix} 0 & 0 & 0 & 0 \\ 0 & 0 & 0 & 0 \\ 0 & 0 & |\epsilon_t|^2 & \epsilon_t^* \\ 0 & 0 & \epsilon_t & \left(1 - \frac{|\epsilon_t|^2}{2}\right) \end{pmatrix}, \quad (71)$$

so that $\Sigma^{u,d} = 0$ if i or $j \neq 3, 4$. This leads to new interesting patterns (in flavor space) of the $\mathcal{H}^0 q_i q_j$ Yukawa

$\tan \beta = 1, \epsilon_t = m_t/m_{t'}$											
Point #	Model	$m_{t'}$	$m_{b'}$	$m_{\nu'}$	$m_{\tau'}$	m_h	m_A	m_H	m_{H^+}	$\sin \theta_{34}$	α
1	4G2HDM-I,II,III	542	358	144	462	260	296	1357	654	0.153	0.74 π
2	4G2HDM-I	511	353	426	455	261	296	1075	428	0.09	0.705 π
3	4G2HDM-I,II,III	548	372	413	434	199	272	1088	707	0.063	1.88 π
4	4G2HDM-I	367	525	829	993	347	491	1227	681	0.011	1.82 π
5	4G2HDM-I	356	537	121	310	675	238	1306	542	0.056	0.97 π
6	4G2HDM-I	440	456	619	634	169	332	405	479	0.082	0.82 π
7 ^a	4G2HDM-I,II,III	526	534	403	420	152	875	550	461	0.007	0.87 π
8	4G2HDM-I	416	510	370	536	216	153	1032	333	0.14	0.96 π
9	4G2HDM-II,III	520	369	738	744	102	882	238	781	0.129	1.28 π
10	4G2HDM-I	500	450	302	414	220	793	1001	750	0.05	$\pi/2$
11	4G2HDM-I	500	450	424	410	120	597	1479	750	0.2	$\pi/2$
12	4G2HDM-I	500	450	147	127	350	716	506	400	0.05	$\pi/2$
13 ^b	4G2HDM-I	450	500	225	235	220	782	303	300	0.2	$\pi/2$
$\tan \beta = 5, \epsilon_t = m_t/m_{t'}$											
14	4G2HDM-II,III	542	386	938	740	126	458	1141	738	0.094	0.9 π
15	4G2HDM-II,III	544	367	305	310	179	417	1255	706	0.117	1.09 π
16	4G2HDM-II,III	517	366	393	211	295	130	1347	801	0.188	0.12 π
17	4G2HDM-II,III	430	412	193	175	246	568	904	617	0.18	0.12 π
18	4G2HDM-II,III	463	451	398	418	170	593	1218	715	0.026	0.25 π
19	4G2HDM-II,III	381	465	545	622	135	145	1084	803	0.051	0.77 π
20	4G2HDM-II,III	514	371	106	610	122	295	1495	819	0.031	1.89 π
21	4G2HDM-II,III	496	399	541	617	148	343	1054	780	0.03	1.77 π
22	4G2HDM-II,III	463	481	959	784	105	319	918	760	0.188	0.03 π
23	4G2HDM-II,III	504	508	497	545	140	118	1175	748	0.166	0.14 π
$\tan \beta = 20, \epsilon_t < 0.1$											
24	4G2HDM-II,III	521	362	178	191	177	231	775	525	0.03	1.96 π
25	4G2HDM-II,III	535	381	568	399	435	573	1500	954	0.073	0.81 π
26	4G2HDM-II,III	542	372	106	314	510	268	1382	450	0.158	0.94 π
27	4G2HDM-II,III	369	527	212	565	571	233	1335	669	0.175	1.88 π
28	4G2HDM-II,III	459	440	684	702	142	455	631	400	0.101	0.12 π
29	4G2HDM-II,III	546	517	260	661	111	216	1347	940	0.186	0.08 π
30	4G2HDM-II,III	411	456	126	423	140	163	1261	940	0.1843	0.11 π

^apoint requires $|\lambda_{sb}^{t'}| \lesssim 10^{-5}$.

^bpoint requires $\epsilon_b \sim m_b/m_{b'}$ in order to have $\text{BR}(b' \rightarrow tH^+) \sim \mathcal{O}(1)$ (see Fig. 19).

TABLE II: List of points (models) in parameter space for our 4G2HDMs of types I, II and III, allowed at 95%CL by PEWD and B-physics flavor data. The 2nd column denotes the model(s) for which the point is applicable. Points 1-3,14-16 and 24 have $m_{t'} - m_{b'} > 150$ GeV with a light CP-even Higgs of mass $m_h \lesssim 300$ GeV, while points 4,5,27 have a large inverted splitting $m_{b'} - m_{t'} > 150$ GeV with a heavier h. Points 6,7 and 17,18,28 have nearly degenerate 4th generation quark and lepton doublets, while points 22,23 have a nearly degenerate 4th generation quark doublet with a lepton doublet heavier than the quark doublet. Points 8,19 have $m_{b'} - m_{t'} > m_W$ and a light charged Higgs, while points 9,16 have $m_{t'} - m_{b'} \sim 150$ GeV with a light Higgs mass of $m_h \sim 100$ GeV. Points 1,8,16,17,22,23,26,27,29,30 all have a large $t' - b/t - b'$ mixing angle: $\theta_{34} \gtrsim 0.15$. Finally, points 10,11 give $\text{BR}(t' \rightarrow th) \sim \mathcal{O}(1)$ (see Fig. 17 in the next section), point 12 gives $\text{BR}(t' \rightarrow bH^+) \sim \mathcal{O}(1)$ (see Fig. 18 in the next section) and point 13 gives $\text{BR}(b' \rightarrow tH^+) \sim \mathcal{O}(1)$ (see Fig. 19 in the next section).

interactions in Eqs. 4-7 ($\mathcal{H}^0 = h, H, A$). In particular, the most notable new features of the 4G2HDM-I are:

1. There are no tree-level FC neutral currents (FCNC) among the quarks of the 1st, 2nd and 3rd generations. That is, no tree-level $c \rightarrow u$, $s \rightarrow d$ transitions, as well as no $t \rightarrow u$, $t \rightarrow c$, $b \rightarrow d$ and $b \rightarrow s$ ones.
2. There are no tree-level FCNC effects involving transitions between the quarks of the 4th generation and the 1st and 2nd generations, i.e., no $t' \rightarrow u$, $t' \rightarrow c$, $b' \rightarrow d$ and $b' \rightarrow s$ transitions. This, makes the 4G2HDM-I compatible with all FCNC constraints coming from light meson mixings and decays, i.e., in the K and D systems.
3. There are new potentially large tree-level FCNC effects in the $\mathcal{H}^0 q_i q_j$ couplings involving the 3rd and 4th generation quarks (i.e., $i, j = 3, 4$), which can have drastic phenomenological consequences for high-energy collider searches of the 4th generation fermions, as we will further discuss below. In particular, the FC $\mathcal{H}' t' t$ and $\mathcal{H}' b' b$ interactions are (taking $\alpha \rightarrow \pi/2$):

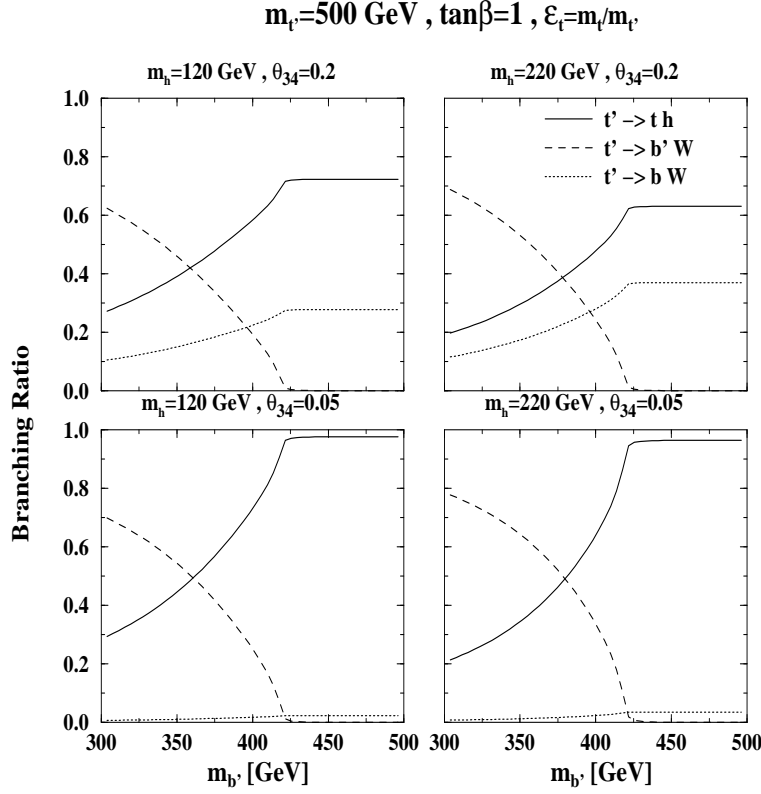


FIG. 17: The branching ratio for the t' decay channels $t' \rightarrow th$, $t' \rightarrow bW$ and $t' \rightarrow b'W^{(*)}$ ($W^{(*)}$ is either on-shell or off-shell depending on the b' mass), as a function of $m_{b'}$ for $m_{t'} = 500 \text{ GeV}$, $\epsilon_t = m_t/m_{t'}$, $\tan\beta = 1$ and $(m_h [\text{GeV}], \theta_{34}) = (120, 0.05), (120, 0.2), (220, 0.05), (220, 0.2)$, as indicated. Also, $\alpha = \pi/2$ and $m_{H^+} > m_{t'}$, $m_A > m_{t'}$ is assumed.

$$\mathcal{L}(ht't) = -\frac{g}{2} \frac{m_{t'}}{m_W} \epsilon_t \sqrt{1+t_\beta^2} \bar{t}' \left(R + \frac{m_t}{m_{t'}} L \right) th, \quad (72)$$

$$\mathcal{L}(Ht't) = -\frac{g}{2} \frac{m_{t'}}{m_W} \epsilon_t \frac{\sqrt{1+t_\beta^2}}{t_\beta} \bar{t}' \left(R + \frac{m_t}{m_{t'}} L \right) tH, \quad (73)$$

$$\mathcal{L}(At't) = i \frac{g}{2} \frac{m_{t'}}{m_W} \epsilon_t \frac{1+t_\beta^2}{t_\beta} \bar{t}' \left(R - \frac{m_t}{m_{t'}} L \right) tA, \quad (74)$$

and similarly for the $\mathcal{H}^0 b'b$ interactions by changing $\epsilon_t \rightarrow \epsilon_b$ (and an extra minus sign in the $Ab'b$ coupling).

We thus see that, if $\epsilon_t \sim m_t/m_{t'}$, then the above couplings can become sizable, e.g., to the level that it might dominate the decay pattern of the t' (see below). In fact, we also expect large FC effects in $b' \rightarrow b$ transitions since, even for a very small $\epsilon_b \sim m_b/m_{b'}$, the FC $hb'b$ and $Ab'b$ Yukawa couplings can become sizable if e.g., $\tan\beta \sim 5$, i.e., in which case they are $\propto \frac{5m_b}{m_W}$.

4. The flavor diagonal interactions of the Higgs species with the up-quarks, $\mathcal{H}^0 uu$, are proportional to $\tan\beta$, thus being a factor of $\tan^2\beta$ larger than the corresponding “conventional” 2HDMs couplings, for which these couplings are $\propto \cot\beta$ (e.g., as in the 2HDM of type II which also underlies the supersymmetric Higgs sector). In particular, the $\mathcal{H}^0 tt$ couplings in our 4G2HDM-I are given by:

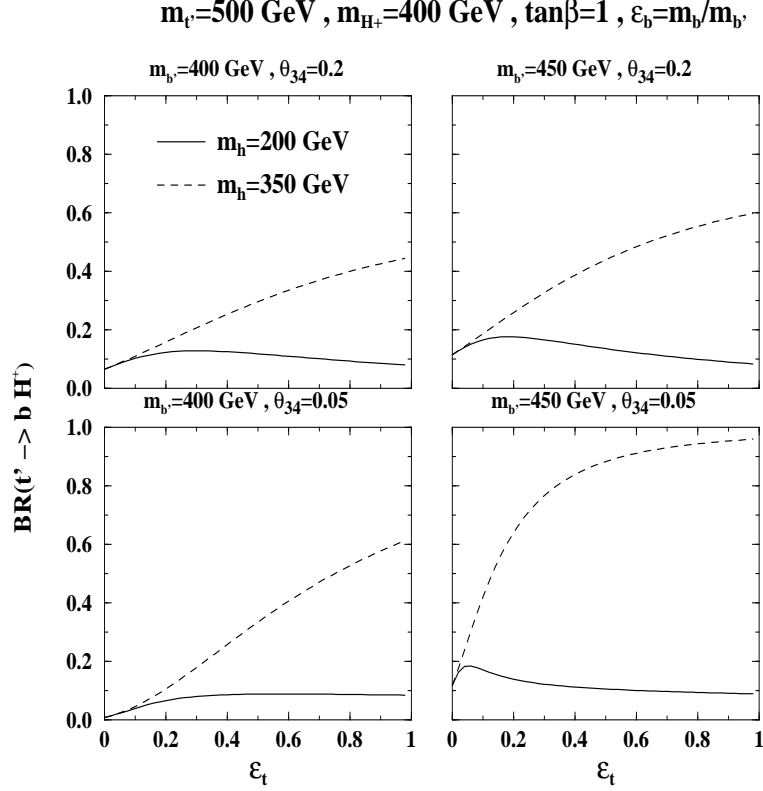


FIG. 18: The branching ratios for the decay $t' \rightarrow bH^+$ as a function of ϵ_t for $m_{t'} = 500 \text{ GeV}$, $m_{H^\pm} = 400 \text{ GeV}$, $\tan\beta = 1$, $\epsilon_b = m_b/m_{b'}$, $m_h = 220$ and 350 GeV and $(m_{b'} [\text{GeV}], \theta_{34}) = (400, 0.05), (400, 0.2), (450, 0.05), (450, 0.2)$, as indicated. Also, $\alpha = \pi/2$ and $m_A > m_{t'}$ is assumed.

$$\mathcal{L}(htt) \approx \frac{g}{2} \frac{m_t}{m_W} \sqrt{1+t_\beta^2} (1-|\epsilon_t|^2) \bar{t}th \xrightarrow{|\epsilon_t|^2 \ll 1} \frac{g}{2} \frac{m_t}{m_W} \sqrt{1+t_\beta^2} \bar{t}th, \quad (75)$$

$$\mathcal{L}(Htt) \approx -\frac{g}{2} \frac{m_t}{m_W} \frac{\sqrt{1+t_\beta^2}}{t_\beta} |\epsilon_t|^2 \bar{t}tH, \quad (76)$$

$$\mathcal{L}(Att) \approx -i \frac{g}{2} \frac{m_t}{m_W} t_\beta \left[1 - (1+t_\beta^{-2}) |\epsilon_t|^2 \right] \bar{t}\gamma_5 tA \xrightarrow{|\epsilon_t|^2 \ll 1} -i \frac{g}{2} \frac{m_t}{m_W} t_\beta \bar{t}\gamma_5 tA. \quad (77)$$

We see that the htt and Att Yukawa interactions are indeed enhanced by a factor of t_β^2 relative to the conventional htt and Att couplings in multi-Higgs models (with no suppression from $t-t'$ mixing parameter ϵ_t). On the other hand, the $ht't'$ and $At't'$ couplings are suppressed by the $t-t'$ mixing parameter and by t_β , respectively:

$$\mathcal{L}(ht't') \approx \frac{g}{4} \frac{m_{t'}}{m_W} \sqrt{1+t_\beta^2} |\epsilon_t|^2 \bar{t}'t'h, \quad (78)$$

$$\mathcal{L}(Ht't') \approx -\frac{g}{2} \frac{m_{t'}}{m_W} \frac{\sqrt{1+t_\beta^2}}{t_\beta} \left(1 - \frac{|\epsilon_t|^2}{2} \right) \bar{t}'t'H, \quad (79)$$

$$\mathcal{L}(At't') \approx -i \frac{g}{2} \frac{m_{t'}}{m_W} t_\beta \left[1 - (1+t_\beta^{-2}) \left(1 - \frac{|\epsilon_t|^2}{2} \right) \right] \bar{t}'\gamma_5 t'A \xrightarrow{|\epsilon_t|^2 \ll 1} i \frac{g}{2} \frac{m_t}{m_W} \frac{1}{t_\beta} \bar{t}\gamma_5 tA. \quad (80)$$

5. The charged Higgs couplings involving the 3rd and 4th generation quarks are completely altered by the presence of the Σ matrix in Eq. 7. For instance, the $H^+t'b$ and H^+tb' couplings have new terms proportional to V_{tb} and

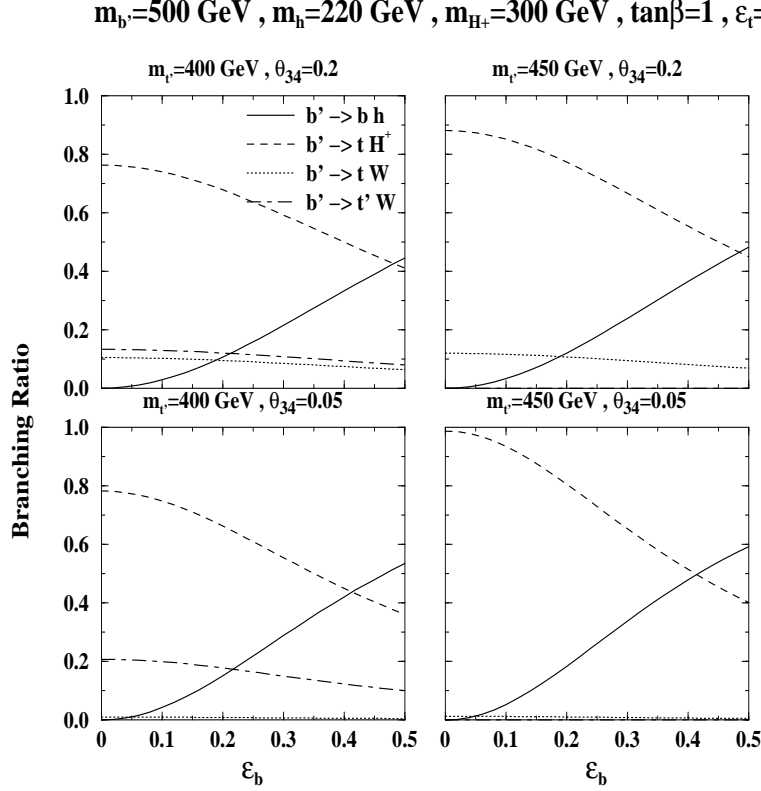


FIG. 19: The branching ratios for the decay channels $b' \rightarrow bh$, $b' \rightarrow tH^+$, $b' \rightarrow tW$ and $b' \rightarrow t'W$, as a function of ϵ_b for $m_{b'} = 500 \text{ GeV}$, $m_h = 220 \text{ GeV}$, $m_{H^+} = 300 \text{ GeV}$, $\tan\beta = 1$, $\epsilon_t = m_t/m_{t'}$ and $(m_{t'} [\text{GeV}], \theta_{34}) = (400, 0.05), (400, 0.2), (450, 0.05), (450, 0.2)$, as indicated. Also, $\alpha = \pi/2$ and $m_A > m_{b'}$ is assumed.

$V_{t'b'}$. In particular, in the “3+1” scenario where $V_{t'd_i}, V_{u_ib'} \rightarrow 0$ for $i = 1, 2, 3$, we have:

$$\mathcal{L}(H^+ t'b) \approx \frac{g}{\sqrt{2}m_W} t_\beta \left(1 + t_\beta^{-2}\right) \bar{t}' (m_t \epsilon_t V_{tb} L - m_{b'} \epsilon_b V_{t'b'} R) b H^+, \quad (81)$$

$$\mathcal{L}(H^+ tb') \approx \frac{g}{\sqrt{2}m_W} t_\beta \left(1 + t_\beta^{-2}\right) \bar{t} (m'_t \epsilon_t^* V_{t'b'} L - m_b \epsilon_b^* V_{tb} R) b' H^+. \quad (82)$$

Recall that in the standard 2HDM of type II that also underlies supersymmetry (assuming four generations of fermions) the $\bar{t}'_R b_L H^+$ would be $\propto m_{t'} V_{t'b}/t_\beta$. We thus see that in our 4G2HDM-I the $\bar{t}'_R b_L H^+$ coupling is potentially enhanced by a factor of $t_\beta^2 \cdot \epsilon_t \cdot (m_t/m_{t'}) \cdot (V_{tb}/V_{t'b})$. For example, if $t_\beta = 3$, $m_{t'} \sim 500 \text{ GeV}$ and $\epsilon_t \sim m_t/m_{t'}$ we get a factor of $V_{tb}/V_{t'b}$ enhancement to the $\bar{t}'_R b_L H^+$ interaction.

The implications of the above new Yukawa interactions can be far reaching with regard to the decay patterns of the t' and the b' and the search strategies for these heavy quarks. In particular, in Fig. 17 we plot the branching ratios of the leading t' decay channels (assuming $m_{H^+}, m_A > m_{t'}$): $t' \rightarrow th$, bW , $b'W^{(*)}$ [$W^{(*)}$ stands for either on-shell or off-shell W depending on the $m_{b'}$], as a function of the b' mass. We use $m_{t'} = 500 \text{ GeV}$, $\tan\beta = 1$, $\epsilon_t = m_t/m_{t'}$ and the following values for m_h and θ_{34} : $(m_h [\text{GeV}], \theta_{34}) = (120, 0.05), (120, 0.2), (220, 0.05), (220, 0.2)$. We see that the $BR(t' \rightarrow th)$ can easily reach $\mathcal{O}(1)$, in particular when $m_{t'} - m_{b'} < m_W$ and even for a rather large $\theta_{34} \sim 0.2$; see e.g., points 10 and 11 in Table II for which $BR(t' \rightarrow th) \sim \mathcal{O}(1)$.

In Fig. 18 we take $m_{H^+} = 400 \text{ GeV}$ (again assuming $m_A > m_{t'}$ so that $t' \rightarrow tA$ is still kinematically closed) and plot $BR(t' \rightarrow bH^+)$ as a function of ϵ_t , for $m_{t'} = 500 \text{ GeV}$, $\tan\beta = 1$, $\epsilon_b = m_b/m_{b'} \sim 0.01$, $m_h = 200$ and 350 GeV and the following values for $m_{b'}$ and θ_{34} ($m_{b'} [\text{GeV}], \theta_{34}) = (400, 0.05), (400, 0.2), (450, 0.05), (450, 0.2)$. We see that the decay channel $t' \rightarrow bH^+$ can become important and even dominate if $\epsilon_t \gtrsim m_t/m_{t'}$, in particular, when $m_{t'} - m_{b'} < m_W$ and a small mixing angle of $\theta_{34} \sim \mathcal{O}(0.05)$; see e.g., point 12 in Table II for which $BR(t' \rightarrow bH^+) \sim \mathcal{O}(1)$.

In Fig. 19 we plot the branching ratios of the leading b' decay channels, as a function of ϵ_b for $m_{b'} = 500$ GeV, $\tan\beta = 1$, $m_{H^+} = 300$ GeV, $m_h = 220$ GeV, $\epsilon_t = m_t/m_{t'}$ and the following values for $m_{t'}$ and θ_{34} ($m_{t'}$ [GeV], θ_{34}) = (400, 0.05), (400, 0.2), (450, 0.05), (450, 0.2). We see that in the b' case the dominance of $b' \rightarrow tH^-$ (if kinematically allowed) is much more pronounced due to the expected smallness of the $b - b'$ mixing parameter, ϵ_b , which controls the FC decay $b' \rightarrow bh$; see e.g., point 13 in Table II for which $BR(b' \rightarrow bH^-) \sim \mathcal{O}(1)$.

This change in the decay pattern of the 4th generation quarks can have important consequences for collider searches of these heavy fermions. For example, as was already noticed in [34], if $t' \rightarrow th$ dominates then t' production at the LHC via $gg \rightarrow t'\bar{t}'$ will lead to the dramatic signature of $t\bar{t}hh$. If $m_h < 2m_W$ (so that h decays to $b\bar{b}$) this will give a $6b + 2W$ signature (i.e., after the top decays via $t \rightarrow bW$), while if $m_h > 2m_W, 2m_Z$ the $t\bar{t}hh$ final state can lead to either $t\bar{t}hh \rightarrow t\bar{t}W^+W^-$ and/or $t\bar{t}hh \rightarrow t\bar{t}ZZ$. In particular, notice that the former $t\bar{t}W^+W^-$ is the one conventionally used for b' searches [32], while the latter will lead to e.g., a $2b + 2W + 4\ell$ signature which is expected to have a rather small irreducible SM-like background (e.g., coming from $gg \rightarrow t\bar{t}h$) that can be further controlled using the kinematic features of the process $gg \rightarrow t'\bar{t}' \rightarrow t\bar{t}hh \rightarrow t\bar{t}ZZ$. If, on the other hand, $t' \rightarrow bH^+$ dominates, then the signature $b\bar{b}H^+H^-$ should be focused on. In this case the t' searches will depend on the H^+ decays, e.g., $H^+ \rightarrow tb$ or $H^+ \rightarrow \tau\nu$, which will lead to $gg \rightarrow t'\bar{t}' \rightarrow 6b + 2W$ or $gg \rightarrow t'\bar{t}' \rightarrow 2b + 2\tau + \cancel{E}_T$, respectively.

For the b' the situation is similar, i.e., the new decays $b' \rightarrow bh$ and/or $b' \rightarrow tH^-$ can also alter the search strategies for b' . For example, if $b' \rightarrow tH^-$ dominates the b' decays, then $gg \rightarrow b'\bar{b}'$ will lead to, e.g., a $t\bar{t}H^-H^+ \rightarrow 4t + 2b$ signature as opposed to the “standard” $2t + 2W$ one when the b' decays via $b' \rightarrow tW$ [90].

Clearly, these new 4th generation quark signatures deserve a detailed investigation which is beyond the scope of this paper and will be considered elsewhere [91].

V. SUMMARY

We have introduced a class of 2HDMs, which we named the 4G2HDM of types I, II and III. Our models are “designed” to give an effective low-energy description for the apparent heaviness of the 4th generation fermions and to address the possibility of dynamical EWSB which is driven by the condensates of these new heavy fermionic states. This is done by giving a special status to the 4th family fermions which are coupled to the scalar doublet that has the heavier VEV. Such setups give rise to very distinct Yukawa textures which can have drastic implications on the phenomenology of 4th generation fermions systems. We studied the constraints from PEWD and from flavor physics in B-systems and outlined the allowed parameter space of our 4G2HDMs, which we find to have various different features than the simpler SM4 version with a single Higgs boson and a 4th family of fermions. For example, we find that the mass splitting $m_{t'} - m_{b'}$ and the inverted mass splitting $m_{b'} - m_{t'}$ can be as large as 200 GeV, and that the mass splitting in the 4th generation lepton doublet can be as large as 400 GeV.

We focused on the 4G2HDM-I, where the Higgs doublet with the heavier VEV is coupled only to the 4th generation doublet while the “lighter” Higgs doublet is coupled to all other quarks. This model is, in our view, somewhat better motivated as it provides a more natural setup in the leptonic sector, i.e., addressing the existence of a 4th generation EW-scale neutrino. In addition, it has very distinctive features in flavor space: there are no tree-level FCNC among the 1st three generation of fermions as well as no FCNC among the 4th generation fermions and the light fermions of the 1st and 2nd generations. On the other hand, the 4G2HDM-I does give rise to potentially large tree-level FCNC $t' \rightarrow t$ and $b' \rightarrow b$ transitions, which, as we briefly explored in the paper, can have significant implications on the search for the 4th generation quarks at high-energy colliders. For example, the FC decay $t' \rightarrow th$ can become the dominant t' decay channel and should therefore effect the search strategy for the t' .

Finally, we note that the 4G2HDM setups can also alter the production and decay patterns of the Higgs particles at hadron colliders. For example, the di-photon Higgs channel $gg \rightarrow h \rightarrow \gamma\gamma$ can be dramatically enhanced or suppressed (to the level of being unobservable at the LHC) compared to the SM4 case. The phenomenology of the production and decay channels of the Higgs particles in the 4G2HDMs will be considered elsewhere.

Acknowledgments: SBS acknowledge research support from the Technion. SN would like to thank Paolo Gambino for useful discussions and the NSERC of Canada for financial support. The work of AS was supported in part by the U.S. DOE contract #DE-AC02-98CH10886(BNL).

-
- [1] E. Lunghi and A. Soni, Phys. Lett. **B666**, 162 (2008).
 - [2] E. Lunghi and A. Soni, JHEP **0908**, 051 (2009).
 - [3] A. Lenz *et al.* [CKMfitter Group], arXiv:1008.1593 [hep-ph].
 - [4] M. Bona *et al.* [UTfit Collaboration], Phys. Lett. B **687**, 61 (2010).

- [5] E. Lunghi and A. Soni, Phys. Rev. Lett. **104**, 251802 (2010).
- [6] E. Lunghi and A. Soni, arXiv:1010.6069 [hep-ph].
- [7] The Heavy Flavor Averaging Group *et al.*, arXiv:1010.1589 [hep-ex].
- [8] V. M. Abazov *et al.* [D0 Collaboration], Phys. Rev. **D82**, 032001 (2010).
- [9] V. M. Abazov *et al.* [D0 Collaboration], Phys. Rev. Lett. **105**, 081801 (2010).
- [10] P.H. Frampton, P.Q. Hung and M. Sher, Phys. Rept. **330**, 263 (2000).
- [11] B. Holdom, W.S. Hou, T. Hurth, M.L. Mangano, S. Sultansoy, G. Unel, talk presented at *Beyond the 3rd SM generation at the LHC era workshop*, Geneva, Switzerland, Sep 2008, arXiv:0904.4698 [hep-ph], published in PMC Phys. **A3**, 4 (2009).
- [12] For older literature on the 4th generation SM, see: Proceedings of the First (February 1987) and the Second (February 1989) International Symposia on the *fourth family of quarks and leptons*, Santa Monica, CA, published in Annals of the New York Academy of Sciences, 517 (1987) & 578 (1989), edited by D. Cline and A. Soni.
- [13] B. Holdom, Phys. Rev. Lett. **57**, 2496 (1986) [Erratum-ibid. **58**, 177 (1987)]; W.A. Bardeen, C.T. Hill and M. Lindner, Phys. Rev. **D41**, 1647 (1990); S.F. King, Phys. Lett. **B234**, 108 (1990); C. Hill, M. Luty and E.A. Paschos, Phys. Rev. **D43**, 3011 (1991); P.Q. Hung and G. Isidori Phys. Lett. **B402**, 122 (1997).
- [14] B. Holdom, JHEP **0608**, 76 (2006).
- [15] P.Q. Hung and Chi Xiong, Nucl. Phys. **B848**, 288 (2011).
- [16] A. Soni, A. K. Alok, A. Giri, R. Mohanta and S. Nandi, Phys. Lett. **B683**, 302 (2010).
- [17] A. Soni, A. K. Alok, A. Giri, R. Mohanta and S. Nandi, Phys. Rev. **D82**, 033009 (2010).
- [18] A. J. Buras, B. Duling, T. Feldmann, T. Heidsieck, C. Promberger and S. Recksiegel, JHEP **1009**, 106 (2010).
- [19] A. J. Buras, B. Duling, T. Feldmann, T. Heidsieck, C. Promberger and S. Recksiegel, JHEP **1007**, 094 (2010).
- [20] W. S. Hou and C. Y. Ma, Phys. Rev. **D82**, 036002 (2010).
- [21] S. Nandi and A. Soni, arXiv:1011.6091 [hep-ph].
- [22] M. Bobrowski, A. Lenz, J. Riedl and J. Rohrwild, Phys. Rev. D **79**, 113006 (2009).
- [23] O. Eberhardt, A. Lenz and J. Rohrwild, Phys. Rev. D **82**, 095006 (2010).
- [24] A.K. Alok, A. Dighe and D. London, arXiv:1011.2634 [hep-ph].
- [25] G. Burdman and L. Da Rold, JHEP **0712**, 86 (2007).
- [26] G. Burdman, L. Da Rold, O. Eboli and R. D’Elia Matheus, Phys. Rev. **D79**, 075026 (2009); G. Burdman, L. de Lima and R.D. Matheus, Phys. Rev. **D83**, 035012 (2011).
- [27] M. Hashimoto and V.A. Miransky, Phys. Rev. **D81**, 055014 (2010).
- [28] W.S. Hou, Chin. J. Phys. **47**, 134 (2009), arXiv:0803.1234 [hep-ph]; W.S. Hou, talk given at *34th International Conference on High Energy Physics (ICHEP 2008)*, Philadelphia, Pennsylvania, Jul 2008, arXiv:0810.3396 [hep-ph].
- [29] C. Jarlskog and R. Stora, Phys. Lett. **B(B)** 208,288,1988; F. del Aguila and J. A. Aguilar-Saavedra, Phys. Lett. **B(B)** 386,241,1996; F. del Aguila and J. A. Aguilar-Saavedra and G. C. Branco, Nucl. Phys. **B510**, 39 (1998).
- [30] S.W. Ham, S.K. Oh, D. Son, Phys. Rev. **D71**, 015001 (2005); R. Fok, G.D. Kribs, Phys. Rev. **D78**, 075023 (2008).
- [31] G. W.S. Hou, arXiv:1101.2161 [hep-ph].
- [32] V.M. Abazov *et al.* (D0 collaboration), arXiv:1104.4522 [hep-ex]; C.J. Flacco, D. Whiteson and M. Kelly, arXiv:1101.4976 [hep-ph]; C.J. Flacco, D. Whiteson, T.M.P. Tait and S. Bar-Shalom, Phys. Rev. Lett. **105**, 111801 (2010); T. Aaltonen *et al.* (CDF collaboration), Phys. Rev. Lett. **104**, 091801 (2010); T. Aaltonen *et al.* (CDF collaboration), Phys. Rev. Lett. **100**, 161803 (2008); A. Lister (CDF collaboration), arXiv:0810.3349 [hep-ex]; J. Conway *et al.* (CDF collaboration), public conference note CDF/PUB/TOP/PUBLIC/10110; D. Whiteson *et al.* (CDF collaboration), CDF public conference note CDF/PUB/TOP/PUBLIC/10243; P. Q. Hung and M. Sher, Phys. Rev. **D77**, 037302 (2008).
- [33] M.A. Luty, Phys. Rev. **D41**, 2893 (1990).
- [34] E. De Pree, G. Marshall and M. Sher, Phys. Rev. **D80**, 037301 (2009).
- [35] P.Q. Hung and Chi Xiong, Nucl. Phys. **B847**, 160 (2011); *ibid.* Phys. Lett. **B694**, 430 (2011).
- [36] M. Hashimoto, Phys. Rev. **D81**, 075023 (2010).
- [37] K. Ishiwata and M.B. Wise, Phys. Rev. **D83**, 074015 (2011).
- [38] J. F. Gunion, H. E. Haber, G. Kane, S. Dawson, “The Higgs Hunter’s Guide”, Addison-Wesley (1990); see also: Errata, SCIPP-92-58 (1992), arXiv:hep-ph/9302272.
- [39] W. Bernreuther, P. Gonzalez, M. Wiebusch, Eur. Phys. J. **C69**, 31 (2010).
- [40] Marc Sher, Phys. Rev. **D61**, 057303 (2000).
- [41] S. Litsey, M. Sher, Phys. Rev. **D80**, 057701 (2009).
- [42] S. Dawson, P. Jaiswal, Phys. Rev. **D82**, 073017 (2010).
- [43] R.C. Cotta, J.L. Hewett, A. Ismail, M.-P. Le, T.G. Rizzo, arXiv:1105.0039 [hep-ph].
- [44] A. Das, C. Kao, Phys. Lett. **B372**, 106 (1996).
- [45] G. Burdman, L. Da Rold, R. D’Elia Matheus, Phys. Rev. **D82**, 055015 (2010).
- [46] K. Agashe, G. Perez, A. Soni, Phys. Rev. **D71**, 016002 (2005).
- [47] S. Casagrande, F. Goertz, U. Haisch, M. Neubert and T. Pfoh, JHEP **0810**, 094 (2008); M. Blanke, A.J. Buras, B. Duling, S. Gori and A. Weiler, JHEP **0903**, 001 (2009).
- [48] For a minimal extension to the SM4 with only one Higgs doublet that can address the heavy 4th generation neutrino problem see, S.F. King, Phys. Lett. **B281**, 295 (1992).
- [49] The Review of Particle Physics, K. Nakamura *et al.* (Particle Data Group), J. Phys. **G37**, 075021 (2010).
- [50] M.E. Peskin, T. Takeuchi, Phys. Rev. Lett. **65**, 964 (1990); *ibid.*, Phys. Rev. **D46**, 381 (1992).
- [51] M. Ciuchini, G. Degrandi, P. Gambino and G. F. Giudice, Nucl. Phys. **B527**, 21 (1998); *ibid.*, Nucl. Phys. **B534**, 3 (1998).
- [52] G. Degrandi, P. Gambino and G. F. Giudice, JHEP **0012**, 009 (2000).

- [53] M. Misiak, S. Pokorski and J. Rosiek, hep-ph/9703442, published in the Review Volume “Heavy Flavors II”, eds. A.J. Buras and M. Lindner, World Scientific Publishing Co., Singapore, 1998.
- [54] K.G. Chetyrkin, M. Misiak and M. Münz, Phys. Lett. **B400**, 206 (1997), [Erratum-ibid. Phys. Lett. **B425**, 414 (1998)].
- [55] C. Greub, T. Hurth and D. Wyler, Phys. Rev. **D54**, 3350 (1996); A.J. Buras, A. Czarnecki, M. Misiak and J. Urban, Nucl. Phys. **B611**, 488 (2001).
- [56] K. G. Chetyrkin, M. Misiak and M. Munz, Phys. Lett. **B400**, 206 (1997); [Erratum-ibid. **B425**, 414 (1998)].
- [57] A. Ali and C. Greub, Phys. Lett. **B361**, 146 (1995).
- [58] N. Pott, Phys. Rev. **D54**, 938 (1996).
- [59] M. Misiak and M. Munz, Phys. Lett. **B344**, 308 (1995).
- [60] K. Adel and Y. P. Yao, Phys. Rev. **D49**, 4945 (1994); C. Greub and T. Hurth, Phys. Rev. **D56**, 2934 (1997); A.J. Buras, A. Kwiatkowski and N. Pott, Nucl. Phys. **B517**, 353 (1998).
- [61] M. Czakon, U. Haisch and M. Misiak, JHEP **0703**, 008 (2007).
- [62] C. Bobeth, M. Misiak and J. Urban, Nucl. Phys. **B574**, 291 (2000).
- [63] A. L. Kagan and M. Neubert, Eur. Phys. J. **C7**, 5 (1999); K. Kiers, A. Soni, G.-H. Wu, Phys. Rev. **D62**, 116004 (2000).
- [64] A. Czarnecki and W. J. Marciano, Phys. Rev. Lett. **81**, 277 (1998).
- [65] K. Baranowski and M. Misiak, Phys. Lett. **B483**, 410 (2000).
- [66] P. Gambino and U. Haisch, JHEP **0009**, 001 (2000).
- [67] M. Misiak, arXiv:0808.3134 [hep-ph].
- [68] A. J. Buras, M. Misiak, M. Munz and S. Pokorski, Nucl. Phys. **B424**, 374 (1994).
- [69] P. Gambino and M. Misiak, Nucl. Phys. **B611**, 338 (2001).
- [70] W. S. Hou and R. S. Willey, Phys. Lett. **B202**, 591 (1988).
- [71] C. Bobeth, M. Misiak and J. Urban, Nucl. Phys. **B567**, 153 (2000).
- [72] A. J. Buras, P. Krawczyk, M. E. Lautenbacher and C. Salazar, Nucl. Phys. **B337**, 284 (1990).
- [73] M.S. Chanowitz, M.A. Furman and I. Hinchliffe, Phys. Lett. **B78**, 285 (1978); *ibid.*, Nucl. Phys. **B153**, 402 (1979).
- [74] E. Gamiz, C. T. H. Davies, G. P. Lepage, J. Shigemitsu and M. Wingate [HPQCD Collaboration], Phys. Rev. **D80**, 014503 (2009).
- [75] E. Gamiz, private communication.
- [76] A. J. Buras, M. Jamin and P. H. Weisz, Nucl. Phys. **B347**, 491 (1990).
- [77] D. Atwood, L. Reina, A. Soni, Phys. Rev. **D54**, 3296 (1996); *ibid.*, Phys. Rev. **D55**, 3156 (1997).
- [78] H.E. Haber, H.E. Logan, Phys. Rev. **D62**, 015011 (2000), and references therein.
- [79] J. Erler, P. Langacker, JHEP **0908**, 017 (2009).
- [80] M.S. Chanowitz, Phys. Rev. **D79**, 113008 (2009).
- [81] See e.g., T. Yanir, JHEP **0206**, 044, (2002); J. Alwall *et al.*, Eur. Phys. J. **C49**, 791 (2007).
- [82] D. Atwood, S. Bar-Shalom, G. Eilam, A. Soni, Phys. Rev. **D66**, 093005 (2002).
- [83] H.-J. He, N. Polonsky, S. Su, Phys. Rev. **D64**, 053004 (2001).
- [84] V.A. Novikov, L.B. Okun, A.N. Rozanov, M.I. Vysotsky, Phys. Lett. **B529**, 111 (2002).
- [85] G. D. Kribs, T. Plehn, M. Spannowsky and T. M. P. Tait, Phys. Rev. **D76**, 075016 (2007).
- [86] J. Erler and P. Langacker, Phys. Rev. Lett. **105**, 031801 (2010).
- [87] M.S. Chanowitz, Phys. Rev. **D82**, 035018 (2010).
- [88] G. Collaboration, <http://gfitter.desy.de/>.
- [89] See e.g., J. Carpenter, R. Norton, S. Siegemund-Broka and A. Soni, Phys. Rev. Lett. **65**, 153 (1990); see also Ref. [10].
- [90] B. Holdom and Q.-S. Yan, arXiv:1101.3844 [hep-ph]; D. Atwood, S.K. Gupta and A. Soni, arXiv:1104.3874 [hep-ph].
- [91] M. Geller, S. Bar-Shalom and G. Eilam, work in progress.